

**Constraints on the late Ediacaran sulfur cycle from carbonate associated sulfate**

Rosalie Tostevin<sup>1\*</sup>, Tianchen He<sup>1</sup>, Alexandra V Turchyn<sup>2</sup>, Rachel A Wood<sup>3</sup>, Amelia M Penny<sup>3</sup>, Fred Bowyer<sup>3</sup>, Gilad Antler<sup>2</sup>, Graham A Shields<sup>1</sup>

<sup>1</sup>*Department of Earth Sciences, University College London, Gower Street, London, WC1E6BT, UK*

<sup>2</sup>*Department of Earth Sciences, University of Cambridge, Downing Street, Cambridge, CB23EQ, UK*

<sup>3</sup>*School of Geosciences, University of Edinburgh, James Hutton Road, Edinburgh, EH93FE, UK*

\*Correspondence to Rosalie Tostevin: rosalie.tostevin@earth.ox.ac.uk. Current address: *Department of Earth Science, University of Oxford, South Parks Road, Oxford, OX14TD, UK*

**Keywords: Sulfur isotopes; Neoproterozoic; Ediacaran; Superheavy pyrite; Method Development; Carbonate-associated sulfate**

**Abstract**

We report new sulfur isotope compositions ( $\delta^{34}\text{S}$ ) in carbonate associated sulfate (CAS) and pyrite from the lower Nama Group, Namibia (~550 to <547 Ma), and use these data to interrogate terminal Ediacaran sulfur cycle dynamics. Our extraction method utilizes an improved pre-leaching procedure that reduces the likelihood of contamination from matrix-bound sulfur. Data generated with the improved

24 extraction method show CAS  $\delta^{34}\text{S}$  as much as 12‰ higher ( $^{34}\text{S}$ -enriched) than  
25 previously reported which suggests a reevaluation of the phenomenon of  
26 'superheavy' pyrite. **The average  $\delta^{34}\text{S}$  of** seawater sulfate increases from 30 to 38‰  
27 in the lower Nama Group, and we correlate this rise in  $\delta^{34}\text{S}$  among  
28 contemporaneous marine basins. Global seawater sulfate  $\delta^{34}\text{S} > 35\text{‰}$  is highly  
29 unusual in Earth history, and in the terminal Ediacaran is best explained by a high  
30 pyrite burial flux. Pyrite in the Nama Group is close in isotopic composition to  
31 coeval sulfate, but the sulfur isotope fractionation between sulfate and pyrite varies  
32 widely among different studied basins, suggesting highly heterogeneous **redox and**  
33 **depositional** conditions.

## 1. Introduction

The hypothesized oxygenation, or ventilation, of the oceans during the Neoproterozoic is of considerable interest because it coincides with the rise of complex animal life (Canfield et al., 2007; Knoll and Sperling, 2014; Runnegar, 1982; Towe, 1970). However, the precise timing and mechanism for this oxygenation, and any causal relationship with animal evolution, remains controversial (Butterfield, 2009; X. Chen et al., 2015; Och and Shields-Zhou, 2012; Sperling et al., 2015). Two of the key fluxes that control the concentration of sulfate in the ocean – riverine sulfate derived from pyrite oxidation, and microbial reduction of sulfate to sulfide – depend indirectly on oxygen concentrations in the atmosphere and oceans, respectively. Furthermore, pyrite burial represents an important source of oxygen to the atmosphere over long timescales (Berner, 1989). Therefore, the biogeochemical sulfur cycle may have been significantly impacted by Neoproterozoic oxygenation. Although higher sulfate concentrations might be expected to correlate with increased oxygen availability, the sulfate concentration of the Neoproterozoic ocean remains unresolved (Fike and Grotzinger, 2008; Loyd et al., 2012; Moles et al., 2015).

The sulfur isotope composition of marine sulfate,  $\delta^{34}\text{S}_{\text{sw}}$ , tracks changes in the sources and sinks within the biogeochemical sulfur cycle (Claypool et al., 1980). The  $\delta^{34}\text{S}_{\text{sw}}$  has varied over Earth history as a result of changes in the riverine sulfate flux, the sulfur isotope composition of the riverine sulfate ( $\delta^{34}\text{S}_{\text{riv}}$ ), the sulfur isotope composition of pyrite ( $\delta^{34}\text{S}_{\text{pyr}}$ ) and the amount of pyrite buried (Berner, 1989;

Claypool et al., 1980; Garrels and Lerman, 1981). Of these various fluxes, the sulfur isotope composition of pyrite and the amount of pyrite buried remain both the largest lever on  $\delta^{34}\text{S}_{\text{sw}}$  as well as the closest link to Earth's surface redox state. Sulfate is respired by sulfate reducing microbes in anoxic environments, producing sulfide which is enriched in  $^{32}\text{S}$  by up to 47‰ or possibly more (Canfield et al., 2010; Leavitt et al., 2013; Sim et al., 2011a, 2011b; Wortmann et al., 2001). In the modern ocean the  $\delta^{34}\text{S}_{\text{sw}}$  is globally homogeneous ( $21.1 \pm 0.8\text{‰}$  when measured via  $\text{SF}_6$ ; Johnston et al., 2014; Rees, 1978).  $\delta^{34}\text{S}_{\text{sw}}$  is elevated over riverine input (which is between 3 and 8 ‰, Canfield, 2013) because of the burial of  $^{32}\text{S}$ -enriched pyrite. Modern marine sulfate has a concentration of 28mM, and a residence time of 10-20 million years, which far exceeds the mixing time of the ocean (Paytan et al., 2004). At high sulfate concentrations,  $\delta^{34}\text{S}_{\text{sw}}$  should provide a globally integrated archive of the relative sources and sinks of sulfur to the global ocean. Marine sulfate concentrations, however, have likely varied widely through Earth history (Hardie, 1996). When the residence time of sulfate is reduced, the concentration and isotope composition of sulfate may vary within and among marine basins (Kah et al., 2004).

Reconstructing  $\delta^{34}\text{S}_{\text{sw}}$  through Earth history requires viable proxy minerals for marine sulfate. Barite ( $\text{BaSO}_4$ ) produced in the open ocean provides a useful archive for the past 150 Ma (the age of the oldest deep sea sediment cores) (e.g. Markovic et al., 2015; Paytan et al., 1998). Barite from the Neoproterozoic, deposited in seafloor exhalative events, has also been used to reconstruct seawater sulfate (Moles et al., 2015; Shields et al., 2007). Calcium sulfate minerals in evaporitic deposits are

80 another viable proxy reservoir (Claypool et al., 1980; Strauss, 1997; Thode and  
81 Monster, 1965), and preserve seawater  $\delta^{34}\text{S}_{\text{sw}}$  with minimal sulfur isotope  
82 fractionation (up to +2.4‰, Raab & Spiro 1991; Thode et al. 1961). However,  
83 evaporitic minerals commonly occur in restricted basins, can be subject to post-  
84 depositional fluid alteration, and suffer from poor chronological constraints  
85 (Bottrell and Newton, 2006). As the gypsum burial flux was limited during periods  
86 of low marine sulfate concentrations (Canfield 2004), there is a dearth of evaporite  
87 deposits in deep time. Trace sulfate in phosphorites has also been shown to  
88 preserve coeval  $\delta^{34}\text{S}_{\text{sw}}$  under some circumstances (Hough et al. 2006; Shields et al.  
89 1999; Shields et al. 2004), but phosphorite deposits are rare on a global scale.  
90  
91 'Carbonate associated sulfate' (CAS) is the most readily available and widely used  
92 proxy for seawater  $\delta^{34}\text{S}_{\text{sw}}$ . CAS is thought to form when a sulfate ion replaces a  
93 carbonate ion in the calcium carbonate mineral structure, and sulfur isotopic  
94 fractionation during incorporation should be negligible (Staudt and Schoonen,  
95 1995). Metastable carbonate minerals undergo recrystallization during diagenesis,  
96 and so may lose their associated sulfate, but original  $\delta^{34}\text{S}_{\text{CAS}}$  values are likely  
97 retained under most conditions (Gill et al., 2008; Kah et al., 2004; Lyons et al., 2004;  
98 Rennie and Turchyn, 2014; Staudt and Schoonen, 1995). The rate and extent of  
99 early diagenetic alteration is in part controlled by the sedimentation rate, the  
100 recrystallisation rate of unstable carbonate minerals, as well as the relative  
101 concentration of sulfate in the pore fluid versus the concentration in the carbonate  
102 minerals (Present et al., 2015; Rennie and Turchyn, 2014).

103

104 Even if  $\delta^{34}\text{S}_{\text{sw}}$  is faithfully preserved in the carbonate record, there are concerns  
105 about the effective extraction of pristine marine phases and imparted contamination  
106 during cleaning and mineral extraction (Peng et al., 2014; Wotte et al., 2012).  
107 Carbonate samples selected for CAS-extraction may be pre-leached to remove  
108 matrix-bound contaminant sulfur, which may include **secondary** atmospheric sulfate  
109 (**SAS**), organic sulfur, or disseminated pyrite, and these generally have a lower  $\delta^{34}\text{S}$ .  
110 Of these various contaminants, one major concern is the oxidation of reduced sulfur  
111 phases such as pyrite, as many studies use bleaches such as NaOCl and  $\text{H}_2\text{O}_2$ , which  
112 can act as effective oxidants (Marenco et al., 2008). It was recently suggested that  
113 SAS results in widespread contamination of  $\delta^{34}\text{S}_{\text{CAS}}$ , particularly in outcrop samples  
114 from arid or heavily polluted regions, as SAS forms a significant component of water  
115 leachable sulfates (Peng et al., 2014). Multiple pre-leaches in 10% NaCl solution are  
116 now suggested for effective cleaning (Theiling and Coleman, 2015; Wotte et al.,  
117 2012), but the pre-leaching procedure is not yet standardized. Pre-leaching that is  
118 less thorough may not eliminate contaminants before the acid-leaching stage,  
119 resulting in acid-leachable sulfate that does not represent primary  $\delta^{34}\text{S}_{\text{sw}}$ .

120

121 Measurements of sulfate  $\delta^{34}\text{S}$  may provide more interpretative power when paired  
122 with coeval pyrite  $\delta^{34}\text{S}$ , which preserves the  $\delta^{34}\text{S}$  signature of the net reduced sulfur  
123 produced during microbial sulfate reduction. Sulfur isotope fractionation during  
124 microbial sulfate reduction,  $^{34}\epsilon_{\text{mic}}$ , depends largely on the rate of microbial sulfate  
125 reduction, which is impacted by other environmental factors, including

temperature, sulfate concentration, the microbial community and organic carbon source (Bradley et al., 2015; Canfield, 2001; Canfield et al., 2010; Habicht and Canfield, 2001; Leavitt et al., 2013; Sim et al., 2011a, 2011b; Wortmann et al., 2001). Pyrite preserves the apparent sulfur isotope fractionation,  $\Delta^{34}\text{S}_{\text{SW-pyr}}$ , which may differ from  $^{34}\epsilon_{\text{mic}}$ , and is controlled by sedimentary parameters including sedimentation rate, porosity, and the availability of reactive organic carbon and reactive iron oxides (Fike et al., 2015). Paired sulfate-pyrite sulfur isotope studies over the Proterozoic show step increases in  $\Delta^{34}\text{S}_{\text{SW-pyr}}$ , which appear to relate closely to changes in the oxidation state of Earth's surface environment (Canfield, 1998; Fike et al., 2006). Existing  $\delta^{34}\text{S}_{\text{SW}}$  records from the Neoproterozoic hint at an interesting evolution of the biogeochemical sulfur cycle towards the Ediacaran - Cambrian boundary. A dramatic rise in  $\delta^{34}\text{S}_{\text{SW}}$  in the latest Ediacaran strata (<541 Ma) has been documented from evaporites and CAS (Claypool et al., 1980; Fike and Grotzinger, 2008; Holser, 1977; Houghton, 1980; Solomon et al., 1971; Strauss et al., 2001). This increase has been interpreted as mixing with deep brines enriched in  $^{34}\text{S}$  through microbial sulfate reduction (Holser, 1977), or a rise in the fractional pyrite burial flux accompanied by increased weathering inputs with elevated  $\delta^{34}\text{S}$  (Fike et al., 2006; Fike and Grotzinger, 2008). The comparatively discontinuous phosphorite record, however, does not show a similar increase in  $\delta^{34}\text{S}_{\text{SW}}$  (cf. Ediacaran data from Shields et al. 2004 and Cambrian data from Shields et al. 1999).

The Nama Group, Namibia is a well-preserved terminal Ediacaran mixed clastic and carbonate succession, deposited between ~550 and 541 Ma (Grotzinger et al., 1995;

Schmitz, 2012). Previous reports of  $\delta^{34}\text{S}_{\text{sw}}$  from the Nama Group reveal an unexpected observation, whereby  $\delta^{34}\text{S}_{\text{pyr}}$  is commonly higher than coeval  $\delta^{34}\text{S}_{\text{CAS}}$  (Ries et al., 2009). This result does not fit within the accepted frameworks for interpreting  $\delta^{34}\text{S}$ , as pyrite typically exhibits lower  $\delta^{34}\text{S}$  compared with coeval sulfate. Sulfide oxidation produces oxidized sulfate that is depleted in  $^{34}\text{S}$  by 4-5‰ (abiotically - Fry et al. 1988), and  $<2\text{‰}$  when microbially mediated (but see Kaplan & Rittenberg 1964 for fractionations up to 18‰), which could in theory leave the residual sulfide pool 'heavy', but in most natural environments this signal would be overprinted by the larger sulfur isotope fractionation during microbial sulfate reduction (Canfield, 2001).

Here, we report high-resolution paired CAS-pyrite sulfur isotope data for the Kuibis Subgroup (~550 to <547 Ma) of the Nama Group, from Zebra River, near Maltahoe, Hardap, Namibia. By applying improved methodologies that minimise the chance of contamination during the cleaning and leaching of carbonate, we produce an improved  $\delta^{34}\text{S}_{\text{CAS}}$  record for the Nama Group. The thorough elimination of contaminants allows us to verify the presence of any 'superheavy' pyrite. We make a detailed comparison between the record from the Nama Group with recent sulfate and pyrite records from contemporaneous basins (Cui et al., 2016; Fike et al., 2006; Fike and Grotzinger, 2008), to assess global trends in the sulfur cycle, marine sulfate concentrations and variability in local redox and depositional conditions.

## 2. Geological and geochemical setting

The Nama Group is a mixed carbonate-siliciclastic sequence deposited in a ramp system across two inter-connected sub-basins, the Witputs in the south and the Zaris in the north, separated by the Osis Arch (figure 1; Germs, 1974). The Nama Group hosts terminal Ediacaran fauna, including soft-bodied fossils belonging to the Ediacaran biota and the skeletal metazoans, *Cloudina*, *Namacalathus* and *Namapoikia* (Grant, 1990; Grotzinger et al., 2000; Hall et al., 2013; Macdonald et al., 2014; Penny et al., 2014, 2016; Wood et al., 2002). Trace fossils have been reported from the Omkyk member (Macdonald et al., 2014), consistent with the beginnings of infaunal bioturbation noted globally during this time (McIlroy and Logan, 1999). Iron speciation data suggest that the Nama Group showed a heterogeneous redox landscape in shallow waters, more persistent oxygenation in most mid-ramp settings, and persistently anoxic and ferruginous in outer ramp waters (Wood et al., 2015).

Our section of the Nama Group, Zebra River Farm, spans the Kuibis Subgroup in the Zaris Basin, and includes the Omkyk and Hoogland Members. Zebra River is a distal inner ramp section, hosting laterally extensive microbial reef systems, and associated skeletal fossils, <35mm (Wood, 2011). Iron speciation data suggest that Zebra River was persistently well-oxygenated, with some restricted anoxic ferruginous periods (Wood et al., 2015). An ash bed in the lowermost Hoogland Member of the Kuibis Subgroup provides robust U–Pb zircon age constraints  $548.8 \pm 1$  Ma (Grotzinger et al. 1995), revised to  $547.36 \pm 0.31$  Ma by Bowring et al.

(2007). The base of the Nama Group is diachronous and has not been well dated, but the age is probably between 548 and 553 Ma, younging towards the Osis Arch (Germs, 1974; Ries et al., 2009). Therefore, the Kuibis Subgroup spans 1-6 Myrs and extends to <547 Ma at the top of the Hoogland member. The inner ramp position of Zebra River means that it may be a relatively late (i.e. young) part of the lower Nama Group.

Previously published carbonate  $\delta^{13}\text{C}$  values from the Nama Group reach as low as -7.4‰ and are interpreted to capture the tail end of the Shuram-Wonoka anomaly (Kaufman et al., 1991; Wood et al., 2015), a large and enigmatic negative carbon isotope excursion recorded globally in Ediacaran carbonates (Burns and Matter, 1993; Calver, 2000; Corsetti and Kaufman, 2003; Lu et al., 2013; McFadden et al., 2008; Saylor et al., 1998). The onset of the carbon isotope excursion is poorly constrained but likely post-dates the Gaskiers glaciation at  $\sim$ 580 Ma (Macdonald et al., 2013). The Shuram anomaly had ended by 551 Ma in South China (Condon et al., 2005). Therefore, the duration of the Shuram event is unknown and could range from 5 to 50 Myrs (Le Guerroué, 2010). The recovery to positive  $\delta^{13}\text{C}$  is likely captured in the southern Witputs Basin (Wood et al., 2015). Elsewhere, the zenith of the negative carbon isotope excursion reaches -12‰, below the  $\delta^{13}\text{C}$  of mantle carbon input, and so demands an exceptional explanation (Grotzinger et al., 2011).

It has been suggested that the Shuram carbon isotope anomaly results from oxidation of a large pool of reduced carbon supplying a substantial amount of  $^{12}\text{C}$  to

the ocean-atmosphere system; this pool of reduced carbon has been suggested to be either methane hydrates (Bjerrum and Canfield, 2011) or dissolved organic carbon (Rothman et al., 2003). This oxidation would, in theory, require a large amount of oxidant, and as such, the  $\delta^{13}\text{C}$  recovery to positive values is interpreted to represent the consumption of the pool of reductant and thus would be expected to be followed by an oxygenation event (Bjerrum and Canfield, 2011; Fike et al., 2006; McFadden et al., 2008; Rothman et al., 2003). One criticism of these models is that they have not considered the massive electron imbalance necessary to sustain the carbon isotope imbalance observed globally for many millions of years, leading others to suggest that the carbon isotope excursion is driven by meteoric or late stage burial diagenesis (Derry, 2010; Knauth and Kennedy, 2009; Swart and Kennedy, 2012). However, these mechanisms are inherently local and cannot explain the globally correlative negative excursion, and recent work has demonstrated that the isotopic signature was present at the time of deposition (Husson et al., 2015). An alternative explanation is global increase in the burial of authigenic carbonate, but this still requires a connection between preserved  $\delta^{13}\text{C}$  and the global DIC reservoir (Schrage et al., 2013).

### 3. Methods

Carbonate samples spanning the Omkyk and Hoogland members of the Kuibis Subgroup were trimmed to remove weathered edges and visible veins, and then rinsed in deionised water. Carbonate rock was crushed and then powdered using an agate mill. The CAS extraction method is an extension / combination of existing

methods (P M Wynn, personal communication; Theiling and Coleman, 2015; Wotte et al., 2012). Approximately 8-10 g of powder was immersed in 10% NaCl solution for five 24-hour leaches under constant agitation, and leachates were rinsed three times in 18 M $\Omega$ cm deionised water between each leach. After each leach, the presence of sulfate released during leaching was tested by adding saturated barium chloride solution (BaCl<sub>2</sub>) to precipitate barite. No barite precipitate was observed after the third leach. Barite from three NaCl pre-leaches was retained and isotopically analysed. The carbonate, once cleaned, was then dissolved in 6M HCl for <20 min. Time exposed to the acid was limited to ensure minimal pyrite oxidation. Acid-leachable sulfate was collected as barite by adding a saturated BaCl<sub>2</sub> solution. Filtrates were cleaned 4 times in ultrapure water and dried before analysis.

Acid volatile sulfur (AVS) and iron sulfide minerals, including pyrite, were chemically extracted using HCl and chromous chloride distillation, respectively, at the University of Leeds. The gas generated during distillation was bubbled through silver nitrate solution to precipitate Ag<sub>2</sub>S (Canfield et al., 1986; Wood et al., 2015). Where sufficient precipitate formed, both AVS and sulfide mineral fractions were retained for analysis. The barite from CAS extraction and silver sulfide from pyrite extraction were weighed into tin cups with an excess of vanadium pentoxide for sulfur isotope analysis at the University of Cambridge. Samples were combusted in a Flash EA coupled through continuous flow through a magnesium perchlorate trap and gas chromatograph before the gas was introduced to a Delta-Advantage mass

spectrometer.  $\delta^{34}\text{S}$  is reported versus the Vienna Canon Diablo Troilite (VCDT) standard. Isotopic barite standards (NBS 127) had an average standard deviation of 0.18‰ ( $1\sigma$ ).  $\delta^{34}\text{S}$  values were corrected for machine drift using this bracketing standard NBS 127 (20.3‰)

The same samples were dissolved in 2% nitric acid, and analysed for major element concentrations (Ca, Mg, Fe, Mn and Sr) using an inductively coupled plasma optical emission spectrometer (ICP-OES) at the Cross-Faculty Elemental Analysis Facility, University College London (see supplementary data file). The concentration of CAS was measured in an aliquot of the filtered acid-leachates, prior to  $\text{BaCl}_2$  addition, via ICP-OES. Wavelength 182.5 was selected to avoid interference with calcium ions, and analysis was conducted using the polyboost function.

#### 4. Results

We present  $\delta^{34}\text{S}_{\text{CAS}}$  from 51 carbonate samples spanning the Omkyk and Hoogland members of the Kuibis Subgroup from the Nama Group, Namibia. The average  $\delta^{34}\text{S}_{\text{CAS}}$  for each member and the standard deviations around the mean are given in table 1. The concentration of  $\text{S}_{\text{CAS}}$  and  $\text{S}_{\text{pyr}}$  in these samples is low, averaging 68.7 ppm (range: 32.6 - 166.6 ppm) and 9.3 ppm (range: <2 - 49.7 ppm), respectively. There is a steady increase in average  $\delta^{34}\text{S}_{\text{CAS}}$  throughout the section (figure 2). The lower Omkyk member averages  $30.1 \pm 5.1\text{‰}$  (range: 21.9 - 39.3‰). The upper Omkyk member averages  $32.3 \pm 3.8\text{‰}$  (range: 26.3 - 39.9‰). The lower Hoogland member averages  $36.4 \pm 4.5\text{‰}$  (range: 27.2 - 41.4‰) and the upper Hoogland member averages  $38.9 \pm 4.1\text{‰}$  (range: 29.7 - 45.4‰).

Sulfur isotope data for pre-leach solutions, measured on the first two leaches for three samples, show lower  $\delta^{34}\text{S}_{\text{NaCl}}$  compared with coeval  $\delta^{34}\text{S}_{\text{CAS}}$  (by as much as 15.8‰) (table 2). This suggests that leaching in NaCl has removed contaminant sulfur, that if unremoved would lower the **apparent**  $\delta^{34}\text{S}_{\text{CAS}}$  value. The final three pre-leaches did not result in sufficient  $\text{BaSO}_4$  precipitate for sulfur isotope analysis, suggesting contaminant sulfur was removed effectively within the first two pre-leaches. The analysed samples from Zebra River show evidence for high-quality preservation, including relatively high  $\delta^{18}\text{O}$  (89% of samples > -10‰), low Mn/Sr ratios (97% of samples <1), and high strontium concentrations (294–5802 ppm; with an average of  $1509 \pm 986$  ppm; 40% of samples >1500 ppm, Wood et al., 2015).

There is no significant covariation between  $\delta^{34}\text{S}_{\text{CAS}}$  and strontium concentrations, Mn/Sr ratios, total organic carbon or total iron (see supplementary data file). We also find that there is no co-variation between  $\delta^{34}\text{S}_{\text{CAS}}$  and cerium or yttrium anomalies measured on the same samples (Tostevin et al., 2016).

We present  $\delta^{34}\text{S}_{\text{pyr}}$  for 11 samples. Pyrite concentrations are low and chromium reduction for many carbonate samples did not produce sufficient pyrite for subsequent sulfur isotope analysis. In the lower Omkyk member, the average  $\delta^{34}\text{S}_{\text{pyr}}$  is  $36.3 \pm 1.8\text{‰}$  (n=5), in the upper Omkyk member  $\delta^{34}\text{S}_{\text{pyr}}$  averages  $31.7 \pm 2.2\text{‰}$  (n=3), and the Hoogland member  $\delta^{34}\text{S}_{\text{pyr}}$  averages  $40.4 \pm 1.5\text{‰}$  (n=3).  $\delta^{34}\text{S}_{\text{pyr}}$  measured on one AVS extraction produced one lower  $\delta^{34}\text{S}_{\text{AVS}}$  ( $26.7\text{‰}$ ) value.

## 5. Discussion

### 5.1 Diagenetic overprinting

Our  $\delta^{34}\text{S}_{\text{CAS}}$  data come from well-described marine sections and have  $\delta^{13}\text{C}$  that can be correlated regionally and globally (Fike et al., 2006; Ries et al., 2009; Wood et al., 2015). Normal marine rare earth element patterns with superchondritic yttrium anomalies throughout the Nama Group further support the interpretation that this section was deposited under open marine conditions (Tostevin et al., 2016).  $\delta^{34}\text{S}_{\text{CAS}}$  shows no correlation with various geochemical indicators of diagenesis, including the concentration of sulfate in the carbonate lattice, Mn/Sr or  $\delta^{18}\text{O}_{\text{CaCO}_3}$  (figure 3), indicating that late-stage diagenetic alteration by non-marine fluids was not the primary controls on  $\delta^{34}\text{S}_{\text{CAS}}$ . However, these traditional parameters for evaluating

diagenesis may not be sufficient to identify syndepositional or early diagenetic alteration in CAS.

We observe sample-to-sample fluctuations from 0.1 to 12.1‰ (average 4.6‰), which are too large to be explained by analytical error or fluctuations in the marine reservoir. Different components of complex carbonate rocks may be differently affected by diagenesis, and so some of the stratigraphic variability in  $\delta^{34}\text{S}_{\text{CAS}}$  may result from facies changes and the leaching of different carbonate components (Present et al., 2015). However, our  $\delta^{34}\text{S}_{\text{CAS}}$  do not appear to correlate with facies or lithology (figure 3). Early diagenetic overprinting, or the incorporation of sulfate into the carbonate lattice during burial and recrystallization, can increase  $\delta^{34}\text{S}_{\text{CAS}}$ , due to microbial sulfate reduction, which through Rayleigh fractionation enriches the pore fluid sulfate in the heavier  $^{34}\text{S}$  isotope. It is also possible for early diagenesis to decrease  $\delta^{34}\text{S}_{\text{CAS}}$ , if recrystallisation or the precipitation of new carbonate minerals occurs close to the chemocline where oxidising fluids interact with sulfide.

Results from modern sediments show that diagenetic alteration of  $\delta^{34}\text{S}_{\text{CAS}}$  is more extensive where high carbonate recrystallization rates intersect with the uppermost zone of sulfate reduction (Rennie and Turchyn, 2014). Pore fluid  $\delta^{34}\text{S}$  evolves to higher values throughout the zone of sulfate reduction while the rate of carbonate recrystallization decreases with age. At rapid sedimentation rates, carbonate recrystallization will occur deeper in the sediment pile, where pore water sulfate

concentrations are low and therefore little isotopically altered sulfate will be incorporated into the carbonate lattice. At slow sedimentation rates, carbonate will undergo intense recrystallization before the onset of sulfate reduction and evolution of pore fluid  $\delta^{34}\text{S}$  so the sulfate incorporated into the carbonate lattice will be minimally evolved from seawater.  $\delta^{34}\text{S}_{\text{CAS}}$  is most vulnerable to resetting at intermediate sedimentation rates, where recrystallization occurs in the presence of sulfate rich, yet isotopically distilled pore fluids (Rennie and Turchyn, 2014). Under modern conditions, diagenesis is unlikely to result in increases in  $\delta^{34}\text{S}_{\text{CAS}}$  greater than 4‰ (Rennie and Turchyn, 2014). However, in the **Ediacaran**, a number of conditions may have enabled greater alteration of  $\delta^{34}\text{S}_{\text{CAS}}$ .

CAS concentrations are exceptionally low in the Nama Group, both compared with modern and Neoproterozoic carbonate rocks from other sections (Gellatly and Lyons, 2005; Staudt and Schoonen, 1995; Strauss et al., 2001). This may be a reflection of the reduced contribution from non-CAS sulfate, due to improved cleaning procedures. Alternately, the low CAS concentrations may result from diagenetic loss, but may also indicate low initial CAS concentrations as a result of a small seawater sulfate reservoir (Berelson et al., 2008; Busenberg and Niel Plummer, 1985; Gill et al., 2008; Marenco et al., 2008). These low concentrations of CAS could increase vulnerability to diagenetic overprinting. However, if sulfate concentrations were very low, this may have **reduced the likelihood of** large sulfur isotope fractionations associated with microbial sulfate reduction (Algeo et al., 2015; Habicht et al., 2002), and this would prevent pore water sulfate from evolving

dramatically away from seawater values. However, we note that large fractionations are still possible at very low sulfate conditions (Canfield et al., 2010; Crowe et al., 2014; Knossow et al., 2015; Weber et al., 2016). Further, sulfate concentrations in pore waters beneath a low-sulfate-concentration water column would also be low, limiting the amount of pore fluid sulfate that could be incorporated during diagenetic recrystallization.

The Nama Group was likely originally aragonite or high Mg calcite, based on original skeletal mineralogies (Zhuravlev and Wood, 2008), modelling trends (Hardie, 2003) and fluid inclusion data (Brennan et al., 2004), and so will have undergone extensive recrystallisation. Gill et al., (2008) show that  $\delta^{34}\text{S}_{\text{CAS}}$  in aragonitic coral heads remained unchanged during meteoric diagenesis and neomorphism to calcite. In contrast, dolomitisation may alter  $\delta^{34}\text{S}_{\text{CAS}}$  by as much as 10‰ (Marenco et al., 2008). More work is needed to fully assess any isotope fractionation during incorporation of sulfur into different carbonate polymorphs. The zone of sulfate reduction may have been shallower in sediments underlying low oxygen waters where there was no penetrative bioturbation. However, the accumulation rate of thrombolite-stromatolite carbonate reef systems may have been very rapid compared to modern carbonate platforms, while the sedimentation rate in the Nama Group overall appears to be exceptionally high at 50-300 mMyr<sup>-1</sup> based on a minimum and maximum age range. Taken together, these differences in Precambrian seawater chemistry and sedimentation patterns, mean that the upper limit for diagenetic alteration is unknown for the Nama Group, but could have

differed **significantly** from the 4‰ limit based on a model derived for modern  
sediments (Rennie and Turchyn, 2014). We conclude that diagenetic alteration  
**likely** explains **most** of the **large** sample-to-sample fluctuations in  $\delta^{34}\text{S}_{\text{CAS}}$ .  
 $\delta^{34}\text{S}_{\text{pyr}}$  reflects the sulfur isotope composition of hydrogen sulfide produced during  
microbial sulfate reduction, or other microbially mediated reactions and depends  
largely on local depositional conditions (e.g. sulfate concentration, iron availability,  
sulfate reduction rate and sedimentation rates) (Canfield 2001; Kaplan & Rittenberg  
1964). Unlike  $\delta^{34}\text{S}_{\text{sw}}$ , which should be globally homogeneous,  $\delta^{34}\text{S}_{\text{pyr}}$  shows a wide  
range of isotope compositions reflecting these local depositional conditions. Some  
pyrite in the Nama Group may have been transformed to iron oxides and aqueous  
sulfate during oxidative weathering (Wood et al., 2015). While this process may  
reduce pyrite concentrations, it should not impact the residual  $\delta^{34}\text{S}_{\text{pyr}}$  (Balci et al.,  
2007).  **$\delta^{34}\text{S}_{\text{pyr}}$  from bulk rock analyses may include late-stage sulfide minerals  
formed during migration of sulfide-bearing fluids through strata rich in reactive  
iron. Detailed petrographic work is needed to identify diagenetic pyrite, and we  
cannot rule out that the  $\delta^{34}\text{S}_{\text{pyr}}$  data reported here have been affected by inclusion of  
late stage sulfide minerals.**

## **5.2 Laboratory extraction of CAS**

Organic sulfur, the products of oxidative pyrite weathering and **secondary  
atmospheric sulfate** (SAS) must all be removed before carbonates are dissolved with  
acid to extract CAS. Previous studies have suggested that the sulfur extracted during

pre-leaching can be as much as 24‰ lower in  $\delta^{34}\text{S}$  than primary CAS (Peng et al., 2014). Cleaning in water has been shown to be inadequate for removing this contaminant matrix-bound sulfur (Peng et al. 2014; Wotte et al. 2012). We have taken care to minimise the possibility of contamination during the extraction of CAS from our samples. We pre-leached five times in 10% NaCl solution under constant agitation, with three rinses in ultrapure water in between each NaCl leach. We used small amounts of powder (8-10 g) in enclosed vessels to minimise any possibility of contamination from within the laboratory. Prior studies on similar sections cleaned large amounts of powder (~300 g) once with Milli-Q water for 24 h before acid leaching, which was common in earlier CAS studies (e.g. Fike et al., 2006; Fike and Grotzinger, 2008; Ries et al., 2009; Zhang et al., 2004, 2003).

We present average  $\delta^{34}\text{S}_{\text{CAS}}$  12.4‰ higher than equivalent samples reported in Ries et al. (2009) for the lower Omkyk member. A common concern during CAS extraction is the inadvertent oxidation of sulfide minerals through the use of oxidants (e.g. NaOCl), or inclusion of matrix bound contaminant sulfur derived from weathered pyrite (Marenco et al., 2008). Disseminated sulfide minerals must have been present in the original rock in concentrations equivalent to or higher than those extracted. Given that measured  $\delta^{34}\text{S}_{\text{pyr}}$  is similar to or even heavier than  $\delta^{34}\text{S}_{\text{CAS}}$ , analytical contamination from pyrite oxidation is unable to lower measured  $\delta^{34}\text{S}_{\text{CAS}}$  by 12‰. The lower apparent CAS values in the Ries et al. (2009) study must therefore originate from the inclusion of the contaminant sulfur that we eliminated during the pre-leaching stage. This  $^{32}\text{S}$  enriched contaminant sulfur (up to 16‰

lower than resultant CAS, table 2), must derive from sources other than pyrite weathering (e.g. SAS). In cases where this sulfate is not effectively removed during pre-leaching, it would contribute to the lower measured CAS sulfur isotope composition.

Our average  $\delta^{34}\text{S}_{\text{CAS}}$  is consistent with Ries et al. (2009) for the upper Omkyk and Hoogland members, but with overall lower standard deviations (table 1). The scatter in their  $\delta^{34}\text{S}_{\text{CAS}}$  may partly result from differing contributions from contaminant phases. There remains significant scatter in our data, however, which is common in CAS data (Bottrell and Newton, 2006; Kampschulte and Strauss, 2004; Rennie and Turchyn, 2014; Turchyn et al., 2009). **SAS, a common contaminant in CAS studies, can accumulate on outer surfaces and microcracks within outcrops, particularly in arid regions such as southern Namibia, and this SAS may be removed by effective cleaning (Peng et al., 2014). However, if SAS is incorporated into secondary carbonate in micro-veins that are impossible to identify and exclude during the powdering process, the contaminant signal would not be removed by pre-leaching and would be included in the acid leachable sulfate fraction. This, along with variable early diagenetic alteration, may explain the remaining scatter in our  $\delta^{34}\text{S}_{\text{CAS}}$  data.**

### **5.3 'Superheavy' pyrite**

There have been several studies investigating the  $\delta^{34}\text{S}$  in various late Neoproterozoic sedimentary successions that report pyrite enriched in  $^{34}\text{S}$  relative

to the global average for seawater sulfate at that time, which is also  $^{34}\text{S}$ -enriched relative to other times in the Proterozoic or Phanerozoic (Bottomley et al., 1992; Liu et al., 2006; Shen et al., 2008; Strauss et al., 1992). This ‘superheavy’ pyrite has also been observed a few times in the Phanerozoic and modern environments, **but the  $\delta^{34}\text{S}_{\text{pyr}}$  is only slightly elevated compared with  $\delta^{34}\text{S}_{\text{CAS}}$  (Aller et al., 2010; Ferrini et al., 2010; Goodfellow and Jonasson, 1984).** On the whole, the occurrence of ‘superheavy’ pyrite involves a small number of anomalously  $^{34}\text{S}$  enriched samples within a larger  $\delta^{34}\text{S}_{\text{pyr}}$  data set, which in some cases are not reported alongside coeval  $\delta^{34}\text{S}_{\text{CAS}}$  (e.g. Bottomley et al. 2009, n=1; Shen et al. 2008, n=4). In particular, Ries et al. (2009) report some extremely  $^{34}\text{S}$ -enriched pyrite in the Hoogland member **(9 samples  $>45.0\text{‰}$ , reaching  $80.2\text{‰}$ ),** but we do not reproduce these in our more limited pyrite data set. **Although our highest reported  $\delta^{34}\text{S}_{\text{CAS}}$  is  $45.4\text{‰}$ , Ries et al. (2009) report some extremely enriched  $\delta^{34}\text{S}_{\text{CAS}}$ , up to  $64.2\text{‰}$ , from the same part of the stratigraphy as the ‘superheavy’ pyrite.**

An apparent ‘superheavy’ pyrite effect may also result from normal marine  $\delta^{34}\text{S}_{\text{pyr}}$ , in the presence of  $\delta^{34}\text{S}_{\text{CAS}}$  that is low compared with contemporaneous local or global sections as a result of contamination during CAS extraction. Our average  $\delta^{34}\text{S}_{\text{CAS}}$  is  $12.4\text{‰}$  higher than equivalent samples reported in Ries et al. (2009) for the lower Omkyk member. Significantly, the lower Omkyk member is one section of the Nama Group where Ries et al. (2009) describe the phenomenon of ‘superheavy’ pyrite (highlighted by the grey box in figure 2). We have not sampled the exact same section as Ries et al. (2009), and so lateral variability in pyrite sulfur isotope

composition or  $\delta^{34}\text{S}_{\text{CAS}}$  across the basin remains a possible explanation (Hurtgen et al., 2006).

Pyrite  $\delta^{34}\text{S}$  remains higher than  $\delta^{34}\text{S}_{\text{CAS}}$  for two samples in the lower Omkyk member and this could point to the presence of genuine 'superheavy' pyrite. Alternately, it could indicate diagenetic alteration of  $\delta^{34}\text{S}_{\text{CAS}}$  to lower values, or the presence of small amounts of contaminant sulfur even after extensive cleaning. In general, our new CAS dataset suggests that 'superheavy' pyrite may not be as widespread in the Nama Group as previously thought (Ries et al. 2009), and that where it does occur, the offset between seawater sulfate and pyrite  $\delta^{34}\text{S}$  may be smaller and therefore easier to explain.

While some of the offset reported in Ries et al. (2009) could have arisen from artifacts during CAS extraction, there remains some extraordinarily high  $\delta^{34}\text{S}_{\text{pyr}}$  in the Nama Group that needs to be addressed. 'Superheavy' pyrite has been attributed to decoupling of surface and bottom water sulfur reservoirs in a stratified ocean, where bottom waters produce enriched  $\delta^{34}\text{S}_{\text{pyr}}$  via Rayleigh distillation, and surface waters record undistilled  $\delta^{34}\text{S}_{\text{CAS}}$  (Liu et al., 2006). This model cannot explain observations in the Nama Group, because there is sedimentological evidence for storm driven mixing in parts of the basin, and iron speciation data suggests there are no sulfidic bottom waters (Ries et al., 2009; Wood et al., 2015). Ries et al. (2009) suggest that under low sulfate conditions, small sulfur isotope fractionations during sulfide oxidation could deplete  $\delta^{34}\text{S}_{\text{sw}}$  in  $^{34}\text{S}$  relative to  $\delta^{34}\text{S}_{\text{pyr}}$  via Rayleigh-type

distillation within pore waters. This interpretation requires **minimal** sulfur isotope fractionation during microbial sulfate reduction, **which may be achieved through very low sulfate concentrations or high rates of sulfate reduction. If pore water sulfide is partially re-oxidised**, aided by storm-driven reworking **or bioturbation beneath aerobic bottom waters, the residual sulfide pool may be left heavy compared with seawater sulfate**. Within the Zebra River section, previous work has identified a spectrum of fully anoxic (ferruginous), low oxygen (manganous) and well-oxygenated bottom waters (Tostevin et al., 2016; Wood et al., 2015). We note that our  $\delta^{34}\text{S}_{\text{CAS}}$  and  $\delta^{34}\text{S}_{\text{pyr}}$  show no **clear** correspondence to **inferred** local bottom water redox conditions.

**Pyrite generally forms within the sediments and so reflects pore water chemistry, whereas carbonate forms close to the sediment-water interface in contact with the marine sulfate reservoir (Gomes and Hurtgen, 2013).  $\delta^{34}\text{S}_{\text{CAS}}$  therefore forms in different environments to  $\delta^{34}\text{S}_{\text{pyr}}$ , decoupling  $\Delta^{34}\text{S}_{\text{SW-pyr}}$  from  $\epsilon^{34}_{\text{mic}}$ .  $\delta^{34}\text{S}_{\text{pyr}}$  may evolve towards parent sulfate  $\delta^{34}\text{S}$  in closed systems, lowering the apparent  $\Delta^{34}\text{S}_{\text{SW-pyr}}$ . The presence of superheavy pyrite may indicate shallow, high energy depositional environments rather than low concentrations of seawater sulfate (Fike et al., 2015). Regardless of the exact mechanism, simple models struggle to explain extremely high  $\delta^{34}\text{S}_{\text{pyr}}$  ( $>50\text{‰}$ ), wide ranges in  $\delta^{34}\text{S}_{\text{pyr}}$ , and the absence of complementary low  $\delta^{34}\text{S}_{\text{pyr}}$ , and so the genesis of ‘superheavy’ pyrite remains enigmatic (Aller et al., 2010; Ferrini et al., 2010; Fike et al., 2015).**

#### 5.4 The terminal Ediacaran Sulfur cycle

Phanerozoic ocean chemistry is dominated by long-term cycles of alternate calcium-rich and magnesium-sulfate-rich seawater (Hardie, 2003, 1996). It is unclear if these trends existed in the Precambrian, but if so, the Ediacaran is projected to be a sulfate-rich 'aragonite' sea (Hardie, 2003). The aragonite and high-Mg calcite original mineralogy of the earliest skeletal metazoans supports this assumption, at least for the final 10 Myrs of the Ediacaran, as well as fluid inclusion data (Brennan et al., 2004; Zhuravlev and Wood, 2008). Superimposed on these potential cyclic trends in the major ion chemistry of the ocean is the hypothesized Neoproterozoic Oxygenation Event, during which higher atmospheric O<sub>2</sub> together with higher rates of physical erosion may have increased sulfate delivery flux, while sinks for reduced sulfur within the ocean did not rise apace. Constraining the concentration of sulfate in the ocean in the past, however, is challenging and controversial (Algeo et al., 2015; Fike et al., 2006; Kah et al., 2004; Loyd et al., 2012).

There are several lines of evidence from previous studies suggesting that marine sulfate concentrations at this time were relatively high. For example, there is evidence that lagoonal waters inside rimmed ocean margins were sulfidic, but not sulfate-limited in South China (Li et al., 2010; Och et al., 2016; Wang et al., 2012).  $\delta^{34}\text{S}$  in some barite deposits appears to be invariant, supporting higher marine sulfate reservoirs (Moles et al., 2015), but the origin of this barite is not demonstrably marine. Limited data from fluid inclusions in evaporite minerals are consistent with high marine sulfate concentrations, although quantifying sulfate

concentrations from fluid inclusions involves large errors and an assumption about the calcium concentration, while the data originate from evaporites that formed in restricted basins (Brennan et al., 2004; Kovalevych et al., 2006). Evaporite deposits are known worldwide from the Ediacaran, including deposits in Oman, India, Russia and Pakistan (Houghton, 1980; Kovalevych et al., 2006; Mattes and Morris, 1990; Strauss et al., 2001). Although the distribution of evaporites through time is predominantly driven by tectonics, the presence of anhydrite in these deposits, where demonstrably marine, requires relatively high sulfate concentrations (several mM) within the Ediacaran-Cambrian transition interval. A rise in  $\Delta^{34}\text{S}_{\text{SW-pyr}}$  during the Neoproterozoic was traditionally interpreted to record a shift towards sulfate reduction combined with sulfur disproportionation in a relatively oxidising environment (Canfield, 1998; Fike et al., 2006). These multiple lines of evidence for high marine sulfate concentrations are contradicted by recent data showing low  $\Delta^{34}\text{S}_{\text{SW-pyr}}$  and rapid rates of change in sulfur isotope composition of proxy minerals, which instead suggest that sulfate concentrations remained low throughout the Neoproterozoic (Algeo et al., 2015; Loyd et al., 2012; Ries et al., 2009). However, reconstructing sulfate concentrations from trends in  $\delta^{34}\text{S}$  requires multiple assumptions, and diagenetic alteration of  $\delta^{34}\text{S}_{\text{CAS}}$  can result in gross underestimates of the marine sulfate reservoir.

#### 5.4.1 Pyrite formation

Sulfur isotopic fractionation during microbial sulfate reduction ( $^{34}\epsilon_{\text{mic}}$ ) is largely associated with intracellular enzymes, but sulfur isotope fractionation may also

572 accompany sulfate transport across the membrane (Rees, 1973).  $^{34}\epsilon_{\text{mic}}$  is a function  
573 of the cell specific sulfate reduction rate, which is in itself dependent on sulfate  
574 concentration, along with other environmental parameters (Canfield, 2001; Habicht  
575 et al., 2005, 2002; Habicht and Canfield, 2001; Leavitt et al., 2013; [Sim et al., 2011a](#)).  
576 More recent work has suggested that large sulfur isotope fractionation can be found  
577 with sulfate concentrations as low as 30  $\mu\text{M}$ , [confounding the simple relationship](#)  
578 [between the magnitude of fractionation and the size of the marine sulfate reservoir](#)  
579 (Canfield et al., 2010; Crowe et al., 2014; Knossow et al., 2015; Weber et al., 2016).  
580 Physiological factors also are important in determining the expressed sulfur isotope  
581 fractionation in any given microbial community (Bradley et al., 2015). Larger  $^{34}\epsilon_{\text{mic}}$   
582 may be expressed in mixed communities in natural environments, where sulfur  
583 undergoes disproportionation and complex recycling, although large sulfur isotope  
584 fractionations have also been recorded during sulfate reduction in pure culture (Sim  
585 et al., 2011a). The largest sulfur isotope fractionations would be expected close to  
586 the chemocline, where oxidation and disproportionation [should \(in theory\)](#) be most  
587 prevalent, but the fractionation has been observed to decrease at redox interfaces in  
588 modern environments (Canfield and Teske, 1996; Fike et al., 2009, 2008; [Wilbanks](#)  
589 [et al., 2014](#)), [so the importance of disproportionation in natural environments is](#)  
590 [unclear](#). In addition, temperature and the carbon source can affect  $^{34}\epsilon_{\text{mic}}$  although  
591 deconvolving whether they impact  $^{34}\epsilon_{\text{mic}}$  or whether they just impact the overall rate  
592 of microbial sulfate reduction is problematic (Canfield 2001; Detmers et al. 2001;  
593 Sim et al. 2011).

594

The broad rise in  $\Delta^{34}\text{S}_{\text{SW-pyr}}$  through the Neoproterozoic could record a switch towards **oxidation and** disproportionation, or a rise in marine sulfate concentrations, both of which would reflect marine oxygenation, but controls on  $\Delta^{34}\text{S}_{\text{SW-pyr}}$  are complex and **other** changes in the marine environment and biosphere could also have impacted  $\Delta^{34}\text{S}_{\text{SW-pyr}}$  (Canfield, 1998; Fike et al., 2006). The expansion of eukaryotes around 800 Ma (Knoll, 2014), and the diversification of animal life 580-520 Ma, and more aerobic water column conditions would have relegated more complex organic carbon molecules to sediments (those which would have escaped oxic respiration), which may have slowed sulfate reduction rates, increasing  $^{34}\epsilon_{\text{mic}}$  (Canfield, 2001; Detmers et al., 2001; Sim et al., 2011b). Furthermore preserved  $\Delta^{34}\text{S}_{\text{SW-pyr}}$  **may differ considerably from  $^{34}\epsilon_{\text{mic}}$  under certain** sedimentation patterns (Fike et al., 2015). Under open system conditions, where pore waters remain in contact with sulfate rich seawater, only a small fraction of the sulfate pool is converted to sulfide during microbial sulfate reduction, and so sulfate concentrations remain high and large  $^{34}\epsilon_{\text{mic}}$  are possible. Under closed system conditions, where pore waters are isolated from seawater, **or where MSR occurs in a sulfate-poor water column**, the sulfate pool may be nearly quantitatively converted to sulfide, and as a result the sulfur isotopes are conserved and the preserved  $\Delta^{34}\text{S}_{\text{SW-pyr}}$  is much smaller **(Gomes and Hurtgen, 2013)**. In summary, the general rise in  $\Delta^{34}\text{S}_{\text{SW-pyr}}$  across the Neoproterozoic does not necessarily have a straightforward relationship with oxygenation and the appearance of oxidation and disproportionation or rising sulfate concentrations and may represent a change in organic carbon or other sedimentary dynamics.

618

619 Despite the general trend of increasing  $\Delta^{34}\text{S}_{\text{SW-pyr}}$  through the Nafun Group in Oman,  
620 in both the overlying Ara Group and the Dengying Formation in South China, local  
621  $\Delta^{34}\text{S}_{\text{SW-pyr}}$  appears to decrease from 50‰ to 30‰ coincident with the first  
622 appearance of *Cloudina* (Cui et al., 2016; Fike and Grotzinger, 2008; Sahoo et al.,  
623 2016). This transition to smaller  $\Delta^{34}\text{S}_{\text{SW-pyr}}$  in younger strata may mark the retreat  
624 of the zone of sulfate reduction into the sediments, and the onset of more closed  
625 system behaviour (Gomes and Hurtgen, 2013). Additional mechanisms to reduce  
626  $\Delta^{34}\text{S}_{\text{SW-pyr}}$  include higher rates of sulfate reduction, possibly driven by changes in  
627 organic carbon availability, the position of the chemocline, lower sulfate  
628 concentrations or temperature (Bradley et al., 2015; Canfield et al., 2010; Canfield,  
629 2001; Habicht and Canfield, 2001; Leavitt et al., 2013; Sim et al., 2011a, 2011b;  
630 Wortmann et al., 2001).

631

632  $\Delta^{34}\text{S}_{\text{SW-pyr}}$  in the Nama Group (<6.6 ‰) is small compared with any of the sulfur  
633 isotope fractionations recorded in Oman and South China, and such small sulfur  
634 isotope fractionations may indicate a microbial-sulfate reduction dominated sulfur  
635 cycle in the presence of low sulfate concentrations, much higher rates of sulfate  
636 reduction locally, or depositional conditions that promoted small preserved  $\Delta^{34}\text{S}_{\text{SW-}}$   
637 *pyr*. The contrasting  $\Delta^{34}\text{S}_{\text{SW-pyr}}$  among basins could be a result of globally  
638 heterogeneous redox conditions in the late Ediacaran, supporting varying amounts  
639 of sulfide re-oxidation and disproportionation. Heterogeneous redox conditions are  
640 supported by differences in local redox proxies, such as Ce anomalies and Fe-

speciation, between the Nama Group and Oman and China (Ling et al., 2013; Och et al., 2016; Schröder and Grotzinger, 2007; Tostevin et al., 2016; Wang et al., 2012; Wood et al., 2015). Complex and localized controls on  $^{34}\epsilon_{\text{mic}}$  and preserved  $\Delta^{34}\text{S}_{\text{sw-pyr}}$  could also cause inter-basin heterogeneity. For example, the presence of Fe(II) in the water column in the Nama Group could have increased the efficiency of the pyrite sink, leading to bulk  $\delta^{34}\text{S}_{\text{pyr}}$  that is close to  $\delta^{34}\text{S}_{\text{sw}}$ . The Nama Group was deposited on a storm dominated carbonate ramp system, where intense reworking or high sedimentation rates may have affected the preserved  $\Delta^{34}\text{S}_{\text{sw-pyr}}$ . The globally heterogeneous  $\Delta^{34}\text{S}_{\text{sw-pyr}}$  in the Ediacaran is a stark warning against a literal interpretation of  $\delta^{34}\text{S}_{\text{pyr}}$  as a record of changes in the global sulfur cycle.

#### 5.4.2 The marine sulfate reservoir

At high marine sulfate concentrations,  $\delta^{34}\text{S}_{\text{sw}}$  and sulfate concentrations should be globally homogeneous across long timescales (>1 Ma), as high concentrations imply large residence times. Rapid temporal changes in  $\delta^{34}\text{S}_{\text{sw}}$  are more likely when sulfate concentrations are lower, as there is more possibility for the  $\delta^{34}\text{S}_{\text{sw}}$  of marine sulfate to be impacted by local processes like river fluxes or to show inter-basin heterogeneity. Using the present day flux of sulfur into and out of the ocean ( $3 \times 10^{12} \text{ mol yr}^{-1}$ ), the calculated sulfate residence time drops below ~100,000 years when sulfate concentrations are less than 0.2 mM, and below ~10,000 years when sulfate concentrations are less than 0.02 mM. A residence time of 10,000 years may have been short enough to permit inter-basin heterogeneity depending on the mixing time of the various ocean basins in the late Ediacaran Period. However,

much about this calculation is unconstrained; for example, the rate of input and output fluxes in the Ediacaran may have been dramatically different from today, with substantially lower oxidative weathering fluxes and higher pyrite burial fluxes.

Rates of change in  $\delta^{34}\text{S}_{\text{sw}}$  are commonly used to estimate the size of the marine sulfate reservoir, assuming that faster rates of change represent a smaller marine sulfate reservoir that can be more easily perturbed over short timescales (Algeo et al., 2015; Kah et al., 2004; Loyd et al., 2012). However, this approach is limited by the inability of most models to account for variations in the  $\delta^{34}\text{S}$  of the input or output fluxes. In these models, the average global isotope offset between sulfate and buried pyrite is often estimated from the recorded  $\Delta^{34}\text{S}_{\text{sw-pyr}}$  in a given section, but  $\Delta^{34}\text{S}_{\text{sw-pyr}}$  varies both temporally and spatially. Further, early diagenesis may alter  $\delta^{34}\text{S}_{\text{CAS}}$  dramatically away from  $\delta^{34}\text{S}_{\text{sw}}$ , as would inclusion of contaminant sulfate in  $\delta^{34}\text{S}_{\text{CAS}}$  analysis. Inclusion of non-meaningful sample-to-sample fluctuations in rate models would lead to drastic underestimates of the size of the seawater sulfate reservoir. A more powerful approach may be to compare  $\delta^{34}\text{S}_{\text{sw}}$  records between marine basins, as  $\delta^{34}\text{S}_{\text{sw}}$  should be globally homogeneous when sulfate concentrations are high. It is therefore important to determine if consistent sulfur isotope records are recorded in geographically separated basins.

The depositional age of the lower Nama Group is well constrained from U-Pb dates from ash beds within the Hoogland Member ( $547.3 \pm 0.3$  Ma - Grotzinger et al. 1995; Schmitz 2012). A rise in  $\delta^{34}\text{S}_{\text{sw}}$  is recorded in limited and poorly age-constrained

data from evaporites in Siberia (Claypool et al., 1980), Iran (Houghton, 1980), India (Strauss et al., 2001) and Australia (Solomon et al., 1971). These data converge on  $\delta^{34}\text{S}$  for seawater sulfate of 30 to 35‰ for the terminal Ediacaran, consistent with data presented here. The Ara Group in the Huqf Supergroup, Oman, can be correlated more precisely using carbon isotope chemostratigraphy and a U-Pb zircon date in the A0 member ( $546.7 \pm 0.3$  Ma; Bowring et al., 2007, Fike et al., 2006; Fike and Grotzinger, 2008; Mattes and Morris, 1990; Morris et al., 1990; Wu et al., 2015; figure 4). The depositional age of the Dengying Formation, South China, is less well constrained, but should be approximately contemporaneous with the Nama Group, based on the presence of *Cloudina* (globally distributed for  $\sim 10$  Myr), carbon isotope chemostratigraphy, detrital zircon ages ( $548 \pm 8$  Ma; Cui et al., 2016; figure 4) and ID-TIMS U-Pb zircon ages for volcanoclastic ash beds ( $< 551 \pm 0.7$  Ma; Condon et al., 2005)

$\delta^{34}\text{S}_{\text{CAS}}$  is high in the Kuibis Subgroup and shows a general rising trend from an average of 30‰ at the base towards an average of 38‰ at the top (figure 2). In Oman, a rapid positive  $\delta^{34}\text{S}_{\text{sw}}$  excursion begins  $\sim 547$  Ma, rising from 30 to 42‰ (Fike & Grotzinger 2008; Wu et al. 2015), dubbed the Ara anomaly. Older parts of the section (the Buah Formation,  $> 547$  Ma), however, record lower  $\delta^{34}\text{S}_{\text{CAS}}$  (20-25‰) compared with the Kuibis Subgroup (Fike et al., 2006). In the Dengying Formation, Zhang et al. (2004) report  $\delta^{34}\text{S}_{\text{CAS}}$  between 20-30‰, in contrast to Y. Chen et al., (2015), who report higher  $\delta^{34}\text{S}_{\text{CAS}}$  between 30-40‰. While these two studies are based on different geographic sections that may record independent

710  $\delta^{34}\text{S}_{\text{sw}}$ , in the Zhang (2004) study, dolostone powders were not cleaned prior to acid  
711 dissolution, and we suggest that the reported  $\delta^{34}\text{S}_{\text{CAS}}$  may have been affected by  
712 inclusion of non-CAS sulfur. Therefore, the Dengying Formation records elevated  
713  $\delta^{34}\text{S}_{\text{sw}}$  consistent with the Nama Group (Y. Chen et al., 2015). This is further  
714 supported by high resolution  $\delta^{34}\text{S}_{\text{CAS}}$  from the Gaojiashan member, in the lower half  
715 of the Dengying Formation (32 to 46‰, Cui et al., 2016, figure 4).

716

717 Carbon isotope chemostratigraphy provides a potentially independent correlation  
718 framework to compare sulfur isotope records. A transition from negative to positive  
719  $\delta^{13}\text{C}$  is recorded in the Buah Formation in Oman, apparently correlative with  $\delta^{13}\text{C}$  in  
720 the Nama Group (see TP2 and TP3 on figure 4). The Zebra River section reaches -  
721 2‰ at the base, but  $\delta^{13}\text{C}$  as low as -7.4‰ are recorded in the directly underlying  
722 member in older parts of the Nama Group (e.g. Brak, see Wood et al., 2015). Using  
723 this correlation framework, the sulfur isotope records among the various published  
724 sections are clearly inconsistent. If the Nama Group and the Huqf Supergroup both  
725 represent open marine conditions, with consistent  $\delta^{13}\text{C}$ , then the residence time of  
726 sulfate must have been very low, permitting spatial variability in  $\delta^{34}\text{S}_{\text{sw}}$  between  
727 basins. One way to reduce the residence time of sulfate is for the sulfate reservoir to  
728 have been small, but sulfate concentrations are hypothesised to be high in the Huqf  
729 Supergroup, to explain the large recorded  $\Delta^{34}\text{S}_{\text{sw-pyr}}$  and fluid inclusion data from  
730 evaporites (Brennan et al., 2004; Fike et al., 2006). The formation of gypsum  
731 evaporite deposits is itself evidence for marine sulfate concentrations of at least  
732 several mM in the upper Ara Group. Alternately, the Huqf Supergroup may have

733 been partially or fully isolated from the global ocean, with an independent  $\delta^{34}\text{S}_{\text{sw}}$   
734 that reflects local inputs or the unidirectional influx of seawater (Wu et al., 2015).  
735 However, there is convincing sedimentological evidence that the Ara evaporites are  
736 marine in nature (Schroder et al., 2004; Schröder et al., 2005, 2003), and a sustained  
737 connection with the global ocean may be required to explain the large volume of  
738 evaporite deposition.

739  
740 Considering the radiometric age constraints, the  $\delta^{34}\text{S}_{\text{CAS}}$  records from Oman, China  
741 and Namibia could potentially be consistent. To reconcile the  $\delta^{34}\text{S}_{\text{CAS}}$  records  
742 between the three sections requires that the lower Nama Group and the Dengying  
743 Formation are contemporaneous with the A0 member in the Ara Group (deposited  
744 between TP1 and TP 2 on figure 4). While the more negative  $\delta^{13}\text{C}$  recorded in parts  
745 of the Nama Group records the recovery from Shuram carbon isotope excursion, the  
746 base of the section is diachronous and the negative  $\delta^{13}\text{C}$  at the base of Zebra River  
747 section may only record the post-Shuram return to more stable conditions (TP1 and  
748 TP2 on figure 4). It is possible that the sulfur isotope records are consistent  
749 between Namibia and Oman, and this supports a rapid and global transition to high  
750  $\delta^{34}\text{S}$  following the termination of the Shuram carbon isotope excursion, as has been  
751 reported elsewhere (Fike and Grotzinger, 2008). We suggest that  $\delta^{34}\text{S}_{\text{sw}}$  climbed  
752 from  $\sim 20\text{‰}$ , close to modern marine sulfate  $\delta^{34}\text{S}$ , to much higher  $\delta^{34}\text{S}$  ( $\sim 40 - 45\text{‰}$   
753 recorded in the Dengying Formation, the Ara Group and the Nama Group) some time  
754 before 547 Ma (Y. Chen et al., 2015; Cui et al., 2016; Fike et al., 2006; Fike and  
755 Grotzinger, 2008; Wu et al., 2015).

756

757 This rise in  $\delta^{34}\text{S}_{\text{CAS}}$  occurred following the termination of the Shuram carbon isotope  
758 excursion, and the marine sulfate  $\delta^{34}\text{S}$  in the terminal Ediacaran is exceptionally  
759 high compared with almost all other periods in Earth history (Claypool et al., 1980).  
760 One mechanism to generate high values for  $\delta^{34}\text{S}_{\text{CAS}}$  is an increase in  $\Delta^{34}\text{S}_{\text{SW-pyr}}$ ,  
761 burying more  $^{32}\text{S}$  enriched pyrite, leaving more  $^{34}\text{S}$  behind in the ocean.  $\Delta^{34}\text{S}_{\text{SW-pyr}}$   
762 varies widely among marine basins, but existing data do not support an increase in  
763 the average global  $\Delta^{34}\text{S}_{\text{SW-pyr}}$  in the terminal Ediacaran; indeed most measured  
764 pyrite is isotopically higher than at other points in time, including in this study (Cui  
765 et al., 2016; Fike and Grotzinger, 2008, figure 4). Elevated  $\delta^{34}\text{S}_{\text{CAS}}$  may instead have  
766 been driven by an increase in the pyrite burial flux,  $f_{\text{py}}$ . Mechanisms to increase  $f_{\text{py}}$   
767 include high sedimentation rates, widespread water column anoxia, high delivery of  
768 iron or high rates of productivity. Increased weathering rates may have delivered  
769 nutrients, driving productivity and simultaneously promoting water column anoxia  
770 (Cui et al., 2016). This weathering flux may additionally have delivered alkalinity  
771 and cations that would have increased carbonate deposition, consistent with the  
772 very high carbonate accumulation rates recorded for the Nama Group (50-300  
773 mMyr<sup>-1</sup>). Fike and Grotzinger, (2008) suggest that changes in the  $\delta^{34}\text{S}$  and flux of  
774 pyrite burial alone cannot explain such elevated  $\delta^{34}\text{S}_{\text{SW}}$ , without the additional  
775 presence of elevated  $\delta^{34}\text{S}_{\text{Riv}}$  (>12‰). One mechanism to elevate  $\delta^{34}\text{S}_{\text{Riv}}$  is the  
776 preferential weathering of sulfates, in the form of evaporite deposits, over sulfide  
777 minerals (Wu et al., 2015). We speculate that high sulfate delivery rates drove some  
778 anoxic basins transiently sulfidic, consistent with local sulfidic conditions reported

for the terminal Ediacaran from China (Och et al., 2016; Wang et al., 2012). This sulfide could have titrated iron from the ocean, resulting in a pulse of pyrite burial, followed by an increase in oxidising power in the oceans.

## Conclusions

We present 51 new  $\delta^{34}\text{S}_{\text{CAS}}$  compositions from the lower Nama Group ( $\sim 550$  -  $<547$  Ma), Namibia. Our data show higher  $\delta^{34}\text{S}_{\text{CAS}}$  than previous studies, which we attribute to improved cleaning procedures and reduced contributions from contaminant sulfur. We suggest that the phenomenon of ‘superheavy’ pyrite, previously reported from these sections, may in part be an artifact of contamination due to inadequate cleaning procedures, and that true  $\delta^{34}\text{S}_{\text{SW}}$  is close to coeval  $\delta^{34}\text{S}_{\text{pyr}}$ . The Nama Group records elevated  $\delta^{34}\text{S}_{\text{SW}}$  and shows a climbing trend from 30‰ to 38‰. This rise in  $\delta^{34}\text{S}_{\text{SW}}$  appears to be recorded globally, suggesting a rapid transition in the sulfur cycle, possibly driven by changing redox conditions and an increase in the pyrite burial flux. The stark contrast in  $\Delta^{34}\text{S}_{\text{SW-pyr}}$  recorded in different sections is consistent with heterogeneous redox or depositional conditions among Ediacaran basins.

## Acknowledgements

RT, GAS and RAW acknowledge financial support from NERC’s Life and the Planet project (NE/1005978/1) and support for isotope analyses came from ERC StG 307582 ‘CARBONSINK’ to AVT. Thanks to Rob Newton for helpful discussions, and Yongbo Peng and David Fike for constructive reviews. Romain Guilbaud and Simon

Poulton assisted with pyrite extractions. We are grateful to L. and G. Fourie for access to Zebra River farm, and Gerd Winterleitner for help with field work.

## References

- Algeo, T.J., Luo, G.M., Song, H.Y., Lyons, T.W., Canfield, D.E., 2015. Reconstruction of secular variation in seawater sulfate concentrations. *Biogeosciences* 12, 2131–2151. doi:10.5194/bg-12-2131-2015
- Aller, R.C., Madrid, V., Chistoserdov, A., Aller, J.Y., Heilbrun, C., 2010. Unsteady diagenetic processes and sulfur biogeochemistry in tropical deltaic muds: Implications for oceanic isotope cycles and the sedimentary record. *Geochimica et Cosmochimica Acta* 74, 4671–4692. doi:10.1016/j.gca.2010.05.008
- Balci, N., Shanks III, W.C., Mayer, B., Mandernack, K.W., 2007. Oxygen and sulfur isotope systematics of sulfate produced by bacterial and abiotic oxidation of pyrite. *Geochimica et Cosmochimica Acta* 71, 3796–3811. doi:10.1016/j.gca.2007.04.017
- Berelson, W., Corsetti, F., Johnson, B., Vo, T., Der, C., 2008. Carbonate-associated sulfate as a proxy for lake level fluctuations: a proof of concept for Walker Lake, Nevada. *J Paleolimnol* 42, 25–36. doi:10.1007/s10933-008-9245-z
- Berner, R.A., 1989. Biogeochemical cycles of carbon and sulfur and their effect on atmospheric oxygen over Phanerozoic time. *Palaeogeography, Palaeoclimatology, Palaeoecology* 75, 97–122. doi:10.1016/0031-0182(89)90186-7
- Bjerrum, C.J., Canfield, D.E., 2011. Towards a quantitative understanding of the late Neoproterozoic carbon cycle. *Proceedings of the National Academy of Sciences* 108, 5542–5547. doi:10.1073/pnas.1101755108
- Bottomley, D.J., Veizer, J., Nielsen, H., Moczydlowska, M., 1992. Isotopic composition of disseminated sulfur in Precambrian sedimentary rocks. *Geochimica et Cosmochimica Acta* 56, 3311–3322.
- Bottrell, S.H., Newton, R.J., 2006. Reconstruction of changes in global sulfur cycling from marine sulfate isotopes. *Earth-Science Reviews* 75, 59–83.
- Bowring, S.A., Grotzinger, J.P., Condon, D.J., Ramezani, J., Newall, M.J., Allen, P.A., 2007. Geochronologic constraints on the chronostratigraphic framework of the Neoproterozoic Huqf Supergroup, Sultanate of Oman. *Am J Sci* 307, 1097–1145. doi:10.2475/10.2007.01
- Bradley, A.S., Leavitt, W.D., Schmidt, M., Knoll, A.H., Girguis, P.R., Johnston, D.T., 2015. Patterns of sulfur isotope fractionation during Microbial Sulfate Reduction. *Geobiology* 14, 91–101. doi:10.1111/gbi.12149
- Brennan, S.T., Lowenstein, T.K., Horita, J., 2004. Seawater chemistry and the advent of biocalcification. *Geology* 32, 473–476. doi:10.1130/G20251.1
- Burns, S.J., Matter, A., 1993. Carbon isotopic record of the latest Proterozoic from Oman. *Eclogae Geologicae Helvetiae*.
- Busenberg, E., Niel Plummer, L., 1985. Kinetic and thermodynamic factors controlling the distribution of  $\text{SO}_3^{2-}$  and  $\text{Na}^+$  in calcites and selected

846 aragonites. *Geochimica et Cosmochimica Acta* 49, 713–725.  
 847 doi:10.1016/0016-7037(85)90166-8  
 848 Butterfield, N.J., 2009. Oxygen, animals and oceanic ventilation: an alternative view.  
 849 *Geobiology* 7, 1–7. doi:10.1111/j.1472-4669.2009.00188.x  
 850 Calver, C.R., 2000. Isotope stratigraphy of the Ediacarian (Neoproterozoic III) of the  
 851 Adelaide Rift Complex, Australia, and the overprint of water column  
 852 stratification. *Precambrian Research* 100, 121–150.  
 853 Canfield, D.E., 2013. Sulfur isotopes in coal constrain the evolution of the  
 854 Phanerozoic sulfur cycle. *Proc. Natl. Acad. Sci. U.S.A.* 110, 8443–8446.  
 855 doi:10.1073/pnas.1306450110  
 856 Canfield, D.E., 2004. The evolution of the Earth surface sulfur reservoir. *American*  
 857 *Journal of Science* 304, 839–861.  
 858 Canfield, D.E., 2001. Isotope fractionation by natural populations of sulfate-reducing  
 859 bacteria. *Geochimica et Cosmochimica Acta* 65, 1117–1124.  
 860 Canfield, D.E., 2001. Biogeochemistry of Sulfur Isotopes. *Reviews in Mineralogy and*  
 861 *Geochemistry* 43, 607–636. doi:10.2138/gsrmg.43.1.607  
 862 Canfield, D.E., 1998. A new model for Proterozoic ocean chemistry. *Nature* 396, 450–  
 863 453. doi:10.1038/24839  
 864 Canfield, D.E., Farquhar, J., Zerkle, A.L., 2010. High isotope fractionations during  
 865 sulfate reduction in a low-sulfate euxinic ocean analog. *Geology* 38, 415–418.  
 866 Canfield, D.E., Poulton, S.W., Narbonne, G.M., 2007. Late-Neoproterozoic Deep-Ocean  
 867 Oxygenation and the Rise of Animal Life. *Science* 315, 92–95.  
 868 doi:10.1126/science.1135013  
 869 Canfield, D.E., Raiswell, R., Westrich, J.T., Reaves, C.M., Berner, R.A., 1986. The use of  
 870 chromium reduction in the analysis of reduced inorganic sulfur in sediments  
 871 and shales. *Chemical Geology* 54, 149–155. doi:10.1016/0009-  
 872 2541(86)90078-1  
 873 Canfield, D.E., Teske, A., 1996. Late Proterozoic rise in atmospheric oxygen  
 874 concentration inferred from phylogenetic and sulphur-isotope studies.  
 875 *Nature* 382, 127–132. doi:10.1038/382127a0  
 876 Chen, X., Ling, H.-F., Vance, D., Shields-Zhou, G.A., Zhu, M., Poulton, S.W., Och, L.M.,  
 877 Jiang, S.-Y., Li, D., Cremonese, L., Archer, C., 2015. Rise to modern levels of  
 878 ocean oxygenation coincided with the Cambrian radiation of animals. *Nat*  
 879 *Commun* 6. doi:10.1038/ncomms8142  
 880 Chen, Y., Chu, X., Zhang, X., Zhai, M., 2015. Carbon isotopes, sulfur isotopes, and trace  
 881 elements of the dolomites from the Dengying Formation in Zhenba area,  
 882 southern Shaanxi: Implications for shallow water redox conditions during  
 883 the terminal Ediacaran. *Sci. China Earth Sci.* 58, 1107–1122.  
 884 doi:10.1007/s11430-015-5071-0  
 885 Claypool, G.E., Holser, W.T., Kaplan, I.R., Sakai, H., Zak, I., 1980. The age curves of  
 886 sulfur and oxygen isotopes in marine sulfate and their mutual interpretation.  
 887 *Chemical Geology* 28, 199–260. doi:10.1016/0009-2541(80)90047-9  
 888 Condon, D., Zhu, M., Bowring, S., Wang, W., Yang, A., Jin, Y., 2005. U-Pb Ages from the  
 889 Neoproterozoic Doushantuo Formation, China. *Science* 308, 95–98.  
 890 doi:10.1126/science.1107765

- Corsetti, F.A., Kaufman, A.J., 2003. Stratigraphic investigations of carbon isotope anomalies and Neoproterozoic ice ages in Death Valley, California. *Geological Society of America Bulletin* 115, 916–932.
- Crowe, S.A., Paris, G., Katsev, S., Jones, C., Kim, S.-T., Zerkle, A.L., Nomosatryo, S., Fowle, D.A., Adkins, J.F., Sessions, A.L., Farquhar, J., Canfield, D.E., 2014. Sulfate was a trace constituent of Archean seawater. *Science* 346, 735–739. doi:10.1126/science.1258966
- Cui, H., Kaufman, A.J., Xiao, S., Peek, S., Cao, H., Min, X., Cai, Y., Siegel, Z., Liu, X.-M., Peng, Y., Schiffbauer, J.D., Martin, A.J., 2016. Environmental context for the terminal Ediacaran biomineralization of animals. *Geobiology*. doi:10.1111/gbi.12178
- Derry, L.A., 2010. A burial diagenesis origin for the Ediacaran Shuram-Wonoka carbon isotope anomaly. *Earth and Planetary Science Letters* 294, 152–162.
- Detmers, J., Bruchert, V., Habicht, K.S., Kuever, J., 2001. Diversity of sulfur isotope fractionations by sulfate-reducing prokaryotes. *Applied and Environmental Microbiology* 67, 888–894.
- Ferrini, V., Fayek, M., De Vito, C., Mignardi, S., Pignatti, J., 2010. Extreme sulphur isotope fractionation in the deep Cretaceous biosphere. *Journal of the Geological Society* 167, 1009–1018.
- Fike, D.A., Bradley, A.S., Rose, C.V., 2015. Rethinking the Ancient Sulfur Cycle. *Annual Review of Earth and Planetary Sciences* 43, 593–622. doi:10.1146/annurev-earth-060313-054802
- Fike, D.A., Finke, N., Zha, J., Blake, G., Hoehler, T.M., Orphan, V.J., 2009. The effect of sulfate concentration on (sub)millimeter-scale sulfide  $\delta^{34}\text{S}$  in hypersaline cyanobacterial mats over the diurnal cycle. *Geochimica et Cosmochimica Acta* 73, 6187–6204. doi:10.1016/j.gca.2009.07.006
- Fike, D.A., Gammon, C.L., Ziebis, W., Orphan, V.J., 2008. Micron-scale mapping of sulfur cycling across the oxycline of a cyanobacterial mat: a paired nanoSIMS and CARD-FISH approach. *ISME J* 2, 749–759. doi:10.1038/ismej.2008.39
- Fike, D.A., Grotzinger, J.P., 2008. A paired sulfate–pyrite  $\delta^{34}\text{S}$  approach to understanding the evolution of the Ediacaran–Cambrian sulfur cycle. *Geochimica et Cosmochimica Acta* 72, 2636–2648. doi:10.1016/j.gca.2008.03.021
- Fike, D.A., Grotzinger, J.P., Pratt, L.M., Summons, R.E., 2006. Oxidation of the Ediacaran Ocean. *Nature* 444, 744–747. doi:10.1038/nature05345
- Fry, B., Ruf, W., Gest, H., Hayes, J., 1988. Sulfur isotope effects associated with oxidation of sulfide by  $\text{O}_2$  in aqueous solution. *Chemical Geology: Isotope Geoscience Section* 73, 205–210.
- Garrels, R.M., Lerman, A., 1981. Phanerozoic cycles of sedimentary carbon and sulfur. *PNAS* 78, 4652–4656.
- Gellatly, A.M., Lyons, T.W., 2005. Trace sulfate in mid-Proterozoic carbonates and the sulfur isotope record of biospheric evolution. *Geochimica et Cosmochimica Acta* 69, 3813–3829. doi:10.1016/j.gca.2005.01.019
- Germis, G.J.B., 1974. The Nama Group in South West Africa and Its Relationship to the Pan-African Geosyncline. *The Journal of Geology* 82, 301–317.

936 Gill, B.C., Lyons, T.W., Frank, T.D., 2008. Behavior of carbonate-associated sulfate  
 937 during meteoric diagenesis and implications for the sulfur isotope  
 938 paleoproxy. *Geochimica et Cosmochimica Acta* 72, 4699–4711.  
 939 doi:10.1016/j.gca.2008.07.001  
 940 Gomes, M.L., Hurtgen, M.T., 2013. Sulfur isotope systematics of a euxinic, low-sulfate  
 941 lake: Evaluating the importance of the reservoir effect in modern and ancient  
 942 oceans. *Geology* 41, 663–666. doi:10.1130/G34187.1  
 943 Goodfellow, W.D., Jonasson, I.R., 1984. Ocean stagnation and ventilation defined by  
 944  $\delta^{34}\text{S}$  secular trends in pyrite and barite, Selwyn Basin, Yukon. *Geology* 12,  
 945 583–586.  
 946 Grant, S.W., 1990. Shell structure and distribution of *Cloudina*, a potential index  
 947 fossil for the terminal Proterozoic. *Am J Sci* 290-A, 261–294.  
 948 Grotzinger, J.P., Bowring, S.A., Saylor, B.Z., Kaufman, A.J., 1995. Biostratigraphic and  
 949 Geochronologic Constraints on Early Animal Evolution. *Science* 270, 598 –  
 950 604. doi:10.1126/science.270.5236.598  
 951 Grotzinger, J.P., Fike, D.A., Fischer, W.W., 2011. Enigmatic origin of the largest-  
 952 known carbon isotope excursion in Earth's history. *Nature Geoscience* 4,  
 953 285–292.  
 954 Grotzinger, J.P., Watters, W.A., Knoll, A.H., 2000. Calcified metazoans in thrombolite-  
 955 stromatolite reefs of the terminal Proterozoic Nama Group, Namibia.  
 956 *Paleobiology* 26, 334 –359. doi:10.1666/0094-  
 957 8373(2000)026<0334:CMITSR>2.0.CO;2  
 958 Habicht, K.S., Canfield, D.E., 2001. Isotope fractionation by sulfate-reducing natural  
 959 populations and the isotopic composition of sulfide in marine sediments.  
 960 *Geology* 29, 555 –558. doi:10.1130/0091-  
 961 7613(2001)029<0555:IFBSRN>2.0.CO;2  
 962 Habicht, K.S., Gade, M., Thamdrup, B., Berg, P., Canfield, D.E., 2002. Calibration of  
 963 Sulfate Levels in the Archean Ocean. *Science* 298, 2372–2374.  
 964 doi:10.1126/science.1078265  
 965 Habicht, K.S., Salling, L., Thamdrup, B., Canfield, D.E., 2005. Effect of low sulfate  
 966 concentrations on lactate oxidation and isotope fractionation during sulfate  
 967 reduction by *Archaeoglobus fulgidus* strain Z. *Applied and environmental*  
 968 *microbiology* 71, 3770–3777.  
 969 Hall, M., Kaufman, A.J., Vickers-Rich, P., Ivantsov, A., Trusler, P., Linnemann, U.,  
 970 Hofmann, M., Elliott, D., Cui, H., Fedonkin, M., others, 2013. Stratigraphy,  
 971 palaeontology and geochemistry of the late Neoproterozoic Aar Member,  
 972 southwest Namibia: Reflecting environmental controls on Ediacara fossil  
 973 preservation during the terminal Proterozoic in African Gondwana.  
 974 *Precambrian Research* 238, 214–232.  
 975 Hardie, L.A., 2003. Secular variations in Precambrian seawater chemistry and the  
 976 timing of Precambrian aragonite seas and calcite seas. *Geology* 31, 785 –788.  
 977 doi:10.1130/G19657.1  
 978 Hardie, L.A., 1996. Secular variation in seawater chemistry: An explanation for the  
 979 coupled secular variation in the mineralogies of marine limestones and  
 980 potash evaporites over the past 600 m.y. *Geology* 24, 279 –283.  
 981 doi:10.1130/0091-7613(1996)024<0279:SVISCA>2.3.CO;2

982 Holser, W.T., 1977. Catastrophic chemical events in the history of the ocean. *Nature*,  
 983 403-408  
 984 Hough, M.L., Shields, G.A., Evins, L.Z., Strauss, H., Henderson, R.A., Mackenzie, S.,  
 985 2006. A major sulphur isotope event at c. 510 Ma: a possible anoxia-  
 986 extinction-volcanism connection during the Early-Middle Cambrian  
 987 transition? *Terra Nova* 18, 257–263. doi:10.1111/j.1365-3121.2006.00687.x  
 988 Houghton, M.L., 1980. *Geochemistry of the Proterozoic Hormuz Evaporites*,  
 989 Southern Iran. University of Oregon.  
 990 Hurtgen, M.T., Halverson, G.P., Arthur, M.A., Hoffman, P.F., 2006. Sulfur cycling in the  
 991 aftermath of a 635-Ma snowball glaciation: Evidence for a syn-glacial sulfidic  
 992 deep ocean. *Earth and Planetary Science Letters* 245, 551–570.  
 993 doi:10.1016/j.epsl.2006.03.026  
 994 Husson, J.M., Higgins, J.A., Maloof, A.C., Schoene, B., 2015. Ca and Mg isotope  
 995 constraints on the origin of Earth's deepest C excursion. *Geochimica et*  
 996 *Cosmochimica Acta* 160, 243–266. doi:10.1016/j.gca.2015.03.012  
 997 Johnston, D., Gill, B., Masterson, A., Beirne, E., Casciotti, K., Knapp, A., Berelson, W.,  
 998 2014. Placing an upper limit on cryptic marine sulphur cycling. *Nature* 513,  
 999 530 - 533. doi 10.1038/nature12719, 530–533.  
 1000 Kah, L.C., Lyons, T.W., Frank, T.D., 2004. Low marine sulphate and protracted  
 1001 oxygenation of the Proterozoic biosphere. *Nature* 431, 834–838.  
 1002 doi:10.1038/nature02974  
 1003 Kampschulte, A., Strauss, H., 2004. The sulfur isotopic evolution of Phanerozoic  
 1004 seawater based on the analysis of structurally substituted sulfate in  
 1005 carbonates. *Chemical Geology* 204, 255–286.  
 1006 doi:10.1016/j.chemgeo.2003.11.013  
 1007 Kaplan, I.R., Rittenberg, S.C., 1964. Microbiological Fractionation of Sulphur  
 1008 Isotopes. *J Gen Microbiol* 34, 195–212. doi:10.1099/00221287-34-2-195  
 1009 Kaufman, A.J., Hayes, J., Knoll, A.H., Germs, G.J., 1991. Isotopic compositions of  
 1010 carbonates and organic carbon from upper Proterozoic successions in  
 1011 Namibia: stratigraphic variation and the effects of diagenesis and  
 1012 metamorphism. *Precambrian Research* 49, 301–327.  
 1013 Knauth, L.P., Kennedy, M.J., 2009. The late Precambrian greening of the Earth.  
 1014 *Nature* 460, 728-732  
 1015 Knoll, A.H., 2014. Paleobiological Perspectives on Early Eukaryotic Evolution. *Cold*  
 1016 *Spring Harb Perspect Biol* 6, a016121. doi:10.1101/cshperspect.a016121  
 1017 Knoll, A.H., Sperling, E.A., 2014. Oxygen and animals in Earth history. *Proceedings of*  
 1018 *the National Academy of Sciences* 111, 3907–3908.  
 1019 Knossow, N., Blonder, B., Eckert, W., Turchyn, A.V., Antler, G., Kamyschny, A., 2015.  
 1020 Annual sulfur cycle in a warm monomictic lake with sub-millimolar sulfate  
 1021 concentrations. *Geochemical Transactions* 16. doi:10.1186/s12932-015-  
 1022 0021-5  
 1023 Kovalevych, V.M., Marshall, T., Peryt, T.M., Petrychenko, O.Y., Zhukova, S.A., 2006.  
 1024 Chemical composition of seawater in Neoproterozoic: Results of fluid  
 1025 inclusion study of halite from Salt Range (Pakistan) and Amadeus Basin  
 1026 (Australia). *Precambrian Research* 144, 39–51.  
 1027 doi:10.1016/j.precamres.2005.10.004

- Leavitt, W.D., Halevy, I., Bradley, A.S., Johnston, D.T., 2013. Influence of sulfate reduction rates on the Phanerozoic sulfur isotope record. *PNAS* 10, 11244 - 11249 doi:10.1073/pnas.1218874110
- Le Guerroué, E., 2010. Duration and synchronicity of the largest negative carbon isotope excursion on Earth: The Shuram/Wonoka anomaly. *Comptes Rendus Geoscience* 342, 204–214. doi:10.1016/j.crte.2009.12.008
- Li, C., Love, G.D., Lyons, T.W., Fike, D.A., Sessions, A.L., Chu, X., 2010. A stratified redox model for the Ediacaran ocean. *Science* 328, 80–83. doi:10.1126/science.1182369
- Ling, H.-F., Chen, X., Li, D., Wang, D., Shields-Zhou, G.A., Zhu, M., 2013. Cerium anomaly variations in Ediacaran–earliest Cambrian carbonates from the Yangtze Gorges area, South China: implications for oxygenation of coeval shallow seawater. *Precambrian Research* 225, 110–127.
- Liu, T.-B., Maynard, J.B., Alten, J., 2006. Superheavy S isotopes from glacier-associated sediments of the Neoproterozoic of south China: Oceanic anoxia or sulfate limitation? *Geological Society of America Memoirs* 198, 205–222.
- Loyd, S.J., Marenco, P.J., Hagadorn, J.W., Lyons, T.W., Kaufman, A.J., Sour-Tovar, F., Corsetti, F.A., 2012. Sustained low marine sulfate concentrations from the Neoproterozoic to the Cambrian: Insights from carbonates of northwestern Mexico and eastern California. *Earth and Planetary Science Letters* 339, 79–94.
- Lu, M., Zhu, M., Zhang, J., Shields-Zhou, G., Li, G., Zhao, F., Zhao, X., Zhao, M., 2013. The DOUNCE event at the top of the Ediacaran Doushantuo Formation, South China: Broad stratigraphic occurrence and non-diagenetic origin. *Precambrian Research, Biogeochemical changes across the Ediacaran-Cambrian transition in South China* 225, 86–109. doi:10.1016/j.precamres.2011.10.018
- Lyons, T.W., Walter, L.M., Gellatly, A.M., Martini, A.M., Blake, R.E., 2004. Sites of anomalous organic remineralization in the carbonate sediments of South Florida, USA: the sulfur cycle and carbonate-associated sulfate. *Geological Society of America Special Papers* 379, 161–176.
- Macdonald, F.A., Pruss, S.B., Strauss, J.V., 2014. Trace fossils with spreiten from the late Ediacaran Nama Group, Namibia: complex feeding patterns five million years before the Precambrian–Cambrian boundary. *Journal of Paleontology* 88, 299–308.
- Macdonald, F.A., Strauss, J.V., Sperling, E.A., Halverson, G.P., Narbonne, G.M., Johnston, D.T., Kunzmann, M., Schrag, D.P., Higgins, J.A., 2013. The stratigraphic relationship between the Shuram carbon isotope excursion, the oxygenation of Neoproterozoic oceans, and the first appearance of the Ediacara biota and bilaterian trace fossils in northwestern Canada. *Chemical Geology* 362, 250–272. doi:10.1016/j.chemgeo.2013.05.032
- Marenco, P.J., Corsetti, F.A., Hammond, D.E., Kaufman, A.J., Bottjer, D.J., 2008. Oxidation of pyrite during extraction of carbonate associated sulfate. *Chemical Geology* 247, 124–132.
- Marenco, P.J., Corsetti, F.A., Kaufman, A.J., Bottjer, D.J., 2008. Environmental and diagenetic variations in carbonate associated sulfate: An investigation of CAS

1074 in the Lower Triassic of the western USA. *Geochimica et Cosmochimica Acta*  
 1075 72, 1570–1582. doi:10.1016/j.gca.2007.10.033  
 1076 Markovic, S., Paytan, A., Wortmann, U.G., 2015. Pleistocene sediment offloading and  
 1077 the global sulfur cycle. *Biogeosciences Discussions* 12, 1205–1245.  
 1078 doi:10.5194/bgd-12-1205-2015  
 1079 Mattes, B.W., Morris, S.C., 1990. Carbonate/evaporite deposition in the Late  
 1080 Precambrian — Early Cambrian Ara Formation of Southern Oman. *Geological*  
 1081 *Society, London, Special Publications* 49, 617–636.  
 1082 doi:10.1144/GSL.SP.1992.049.01.37  
 1083 McFadden, K.A., Huang, J., Chu, X., Jiang, G., Kaufman, A.J., Zhou, C., Yuan, X., Xiao, S.,  
 1084 2008. Pulsed oxidation and biological evolution in the Ediacaran Doushantuo  
 1085 Formation. *Proceedings of the National Academy of Sciences* 105, 3197–  
 1086 3202.  
 1087 McIlroy, D., Logan, G.A., 1999. The impact of bioturbation on infaunal ecology and  
 1088 evolution during the Proterozoic–Cambrian transition. *Palaaios* 14, 58–72.  
 1089 Miller, R.M., 1983. The Pan-African Damara Orogen of South West Africa/Namibia.  
 1090 Moles, N.R., Boyce, A.J., Fallick, A.E., 2015. Abundant sulphate in the Neoproterozoic  
 1091 ocean: implications of constant  $\delta^{34}\text{S}$  of barite in the Aberfeldy SEDEX  
 1092 deposits, Scottish Dalradian. *Geological Society, London, Special Publications*  
 1093 393, 189–212. doi:10.1144/SP393.7  
 1094 Morris, S.C., Mattes, B., Chen, M., 1990. The early skeletal organism *Cloudina*: new  
 1095 occurrences from Oman and possibly China. *American Journal of Science*  
 1096 245–260.  
 1097 Och, L.M., Cremonese, L., Shields-Zhou, G.A., Poulton, S.W., Struck, U., Ling, H., Li, D.,  
 1098 Chen, X., Manning, C., Thirlwall, M., Strauss, H., Zhu, M., 2016.  
 1099 Palaeoceanographic controls on spatial redox distribution over the Yangtze  
 1100 Platform during the Ediacaran–Cambrian transition. *Sedimentology* 63, 378–  
 1101 410. doi:10.1111/sed.12220  
 1102 Och, L.M., Shields-Zhou, G.A., 2012. The Neoproterozoic oxygenation event:  
 1103 environmental perturbations and biogeochemical cycling. *Earth-Science*  
 1104 *Reviews* 110, 26–57.  
 1105 Paytan, A., Kastner, M., Campbell, D., Thiemens, M.H., 2004. Seawater Sulfur Isotope  
 1106 Fluctuations in the Cretaceous. *Science* 304, 1663–1665.  
 1107 doi:10.1126/science.1095258  
 1108 Paytan, A., Kastner, M., Campbell, D., Thiemens, M.H., 1998. Sulfur Isotopic  
 1109 Composition of Cenozoic Seawater Sulfate. *Science* 282, 1459–1462.  
 1110 doi:10.1126/science.282.5393.1459  
 1111 Peng, Y., Bao, H., Pratt, L.M., Kaufman, A.J., Jiang, G., Boyd, D., Wang, Q., Zhou, C., Yuan,  
 1112 X., Xiao, S., Loyd, S., 2014. Widespread contamination of carbonate-associated  
 1113 sulfate by present-day secondary atmospheric sulfate: Evidence from triple  
 1114 oxygen isotopes. *Geology* 42, 815–818.  
 1115 Penny, A.M., Wood, R.A., Zhuravlev, A.Y., Curtis, A., Bowyer, F., Tostevin, R., 2016.  
 1116 Intraspecific variation in an Ediacaran skeletal metazoan: *Namacalathus* from  
 1117 the Nama Group, Namibia. *Geobiology*. doi:10.1111/gbi.12205

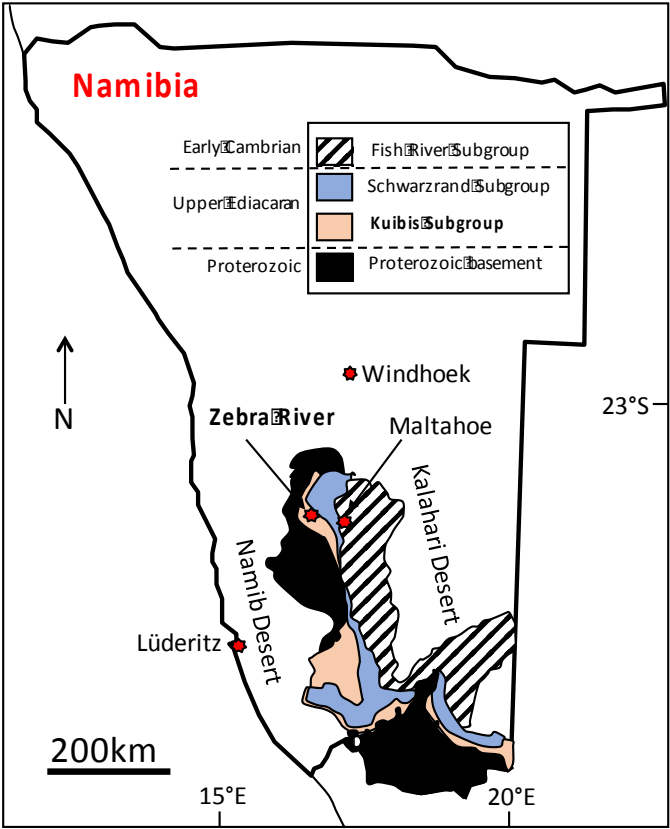
1118 Penny, A., Wood, R., Curtis, A., Bowyer, F., Tostevin, R., Hoffman, K.-H., 2014.  
 1119 Ediacaran metazoan reefs from the Nama Group, Namibia. *Science* 344,  
 1120 1504–1506.  
 1121 Present, T.M., Paris, G., Burke, A., Fischer, W.W., Adkins, J.F., 2015. Large Carbonate  
 1122 Associated Sulfate isotopic variability between brachiopods, micrite, and  
 1123 other sedimentary components in Late Ordovician strata. *Earth and*  
 1124 *Planetary Science Letters* 432, 187–198. doi:10.1016/j.epsl.2015.10.005  
 1125 Raab, M., Spiro, B., 1991. Sulfur isotopic variations during seawater evaporation  
 1126 with fractional crystallization. *Chemical Geology: Isotope Geoscience section*  
 1127 86, 323–333. doi:10.1016/0168-9622(91)90014-N  
 1128 Rees, C.E., 1978. Sulphur isotope measurements using SO<sub>2</sub> and SF<sub>6</sub>. *Geochimica et*  
 1129 *Cosmochimica Acta* 42, 383–389. doi:10.1016/0016-7037(78)90269-7  
 1130 Rees, C.E., 1973. A steady-state model for sulphur isotope fractionation in bacterial  
 1131 reduction processes. *Geochimica et Cosmochimica Acta* 37, 1141–1162.  
 1132 doi:10.1016/0016-7037(73)90052-5  
 1133 Rennie, V.C.F., Turchyn, A.V., 2014. The preservation of and in carbonate-associated  
 1134 sulfate during marine diagenesis: A 25 Myr test case using marine sediments.  
 1135 *Earth and Planetary Science Letters* 395, 13–23.  
 1136 doi:10.1016/j.epsl.2014.03.025  
 1137 Ries, J.B., Fike, D.A., Pratt, L.M., Lyons, T.W., Grotzinger, J.P., 2009. Superheavy pyrite  
 1138 ( $\delta^{34}\text{S}_{\text{pyr}} > \delta^{34}\text{S}_{\text{SCAS}}$ ) in the terminal Proterozoic Nama Group, southern  
 1139 Namibia: A consequence of low seawater sulfate at the dawn of animal life.  
 1140 *Geology* 37, 743–746. doi:10.1130/G25775A.1  
 1141 Rothman, D.H., Hayes, J.M., Summons, R.E., 2003. Dynamics of the Neoproterozoic  
 1142 carbon cycle. *PNAS* 100, 8124–8129. doi:10.1073/pnas.0832439100  
 1143 Runnegar, B., 1982. Oxygen requirements, biology and phylogenetic significance of  
 1144 the late Precambrian worm Dickinsonia, and the evolution of the burrowing  
 1145 habit. *Alcheringa: An Australasian Journal of Palaeontology* 6, 223–239.  
 1146 doi:10.1080/03115518208565415  
 1147 Sahoo, S.K., Planavsky, N.J., Jiang, G., Kendall, B., Owens, J.D., Wang, X., Shi, X., Anbar,  
 1148 A.D., Lyons, T.W., 2016. Oceanic oxygenation events in the anoxic Ediacaran  
 1149 ocean. *Geobiology*. doi:10.1111/gbi.12182  
 1150 Saylor, B.Z., Kaufman, A.J., Grotzinger, J.P., Urban, F., 1998. A Composite Reference  
 1151 Section for Terminal Proterozoic Strata of Southern Namibia. *SEPM Journal of*  
 1152 *Sedimentary Research* 68. doi:10.1306/D426893C-2B26-11D7-  
 1153 8648000102C1865D  
 1154 Schmitz, M.D., 2012. Radiogenic isotope geochronology. *Geologic Time Scale* 115–  
 1155 126.  
 1156 Schrag, D.P., Higgins, J.A., Macdonald, F.A., Johnston, D.T., 2013. Authigenic carbonate  
 1157 and the history of the global carbon cycle. *science* 339, 540–543.  
 1158 Schröder, S., Grotzinger, J. P., 2007. Evidence for anoxia at the Ediacaran–Cambrian  
 1159 boundary: the record of redox-sensitive trace elements and rare earth  
 1160 elements in Oman. *Journal of the Geological Society* 164, 175–187.  
 1161 doi:10.1144/0016-76492005-022  
 1162 Schröder, S., Grotzinger, J.P., Amthor, J.E., Matter, A., 2005. Carbonate deposition and  
 1163 hydrocarbon reservoir development at the Precambrian–Cambrian

1164 boundary: The Ara Group in South Oman. *Sedimentary Geology* 180, 1–28.  
 1165 doi:10.1016/j.sedgeo.2005.07.002  
 1166 Schröder, S., Schreiber, B.C., Amthor, J.E., Matter, A., 2003. A depositional model for  
 1167 the terminal Neoproterozoic–Early Cambrian Ara Group evaporites in south  
 1168 Oman. *Sedimentology* 50, 879–898. doi:10.1046/j.1365-3091.2003.00587.x  
 1169 Schroder, S., Schreiber, C., Amthor, J.E., Matter, A., 2004. Stratigraphy and  
 1170 environmental conditons of the terminal Neoproterozoic - Cambrian period  
 1171 in Oman: evidence from sulphur isotopes. *Journal of the Geological Society*  
 1172 161, 489–499.  
 1173 Shen, Y., Zhang, T., Hoffman, P.F., 2008. On the coevolution of Ediacaran oceans and  
 1174 animals. *Proceedings of the National Academy of Sciences* 105, 7376–7381.  
 1175 Shields, G.A., Deynoux, M., Strauss, H., Paquet, H., Nahon, D., 2007. Barite-bearing cap  
 1176 dolostones of the Taoudéni Basin, northwest Africa: Sedimentary and  
 1177 isotopic evidence for methane seepage after a Neoproterozoic glaciation.  
 1178 *Precambrian Research* 153, 209–235. doi:10.1016/j.precamres.2006.11.011  
 1179 Shields, G.A., Strauss, H., Howe, S.S., Siegmund, H., 1999. Sulphur isotope  
 1180 compositions of sedimentary phosphorites from the basal Cambrian of China:  
 1181 implications for Neoproterozoic-Cambrian biogeochemical cycling. *Journal of*  
 1182 *the Geological Society* 156, 943–955.  
 1183 Shields, G., Kimura, H., Yang, J., Gammon, P., 2004. Sulphur isotopic evolution of  
 1184 Neoproterozoic-Cambrian seawater: new francolite-bound sulphate  $\delta^{34}\text{S}$  data  
 1185 and a critical appraisal of the existing record. *Chemical Geology* 204, 163–  
 1186 182.  
 1187 Sim, M.S., Bosak, T., Ono, S., 2011a. Large Sulfur Isotope Fractionation Does Not  
 1188 Require Disproportionation. *Science* 333, 74–77.  
 1189 doi:10.1126/science.1205103  
 1190 Sim, M.S., Ono, S., Donovan, K., Templer, S.P., Bosak, T., 2011b. Effect of electron  
 1191 donors on the fractionation of sulfur isotopes by a marine *Desulfovibrio* sp.  
 1192 *Geochimica et Cosmochimica Acta* 75, 4244–4259.  
 1193 doi:10.1016/j.gca.2011.05.021  
 1194 Solomon, M., Rafter, T.A., Dunham, K.C., 1971. Sulphur and oxygen isotope studies in  
 1195 the northern Pennines in relation to ore diagenesis. *Transactions of the*  
 1196 *Institution of Mining and Metallurgy* 259–275.  
 1197 Sperling, E.A., Wolock, C.J., Morgan, A.S., Gill, B.C., Kunzmann, M., Halverson, G.P.,  
 1198 Macdonald, F.A., Knoll, A.H., Johnston, D.T., 2015. Statistical analysis of iron  
 1199 geochemical data suggests limited late Proterozoic oxygenation. *Nature* 523,  
 1200 451–454. doi:10.1038/nature14589  
 1201 Staudt, W.J., Schoonen, M.A., 1995. Sulfate incorporation into sedimentary  
 1202 carbonates, in: *ACS Symposium Series*. Washington, DC: American Chemical  
 1203 Society, 332–347.  
 1204 Strauss, H., 1997. The isotopic composition of sedimentary sulfur through time.  
 1205 *Palaeogeography, Palaeoclimatology, Palaeoecology* 132, 97–118.  
 1206 doi:10.1016/S0031-0182(97)00067-9  
 1207 Strauss, H., Banerjee, D.M., Kumar, V., 2001. The sulfur isotopic composition of  
 1208 Neoproterozoic to early Cambrian seawater—evidence from the cyclic  
 1209 Hanseran evaporites, NW India. *Chemical Geology* 175, 17–28.

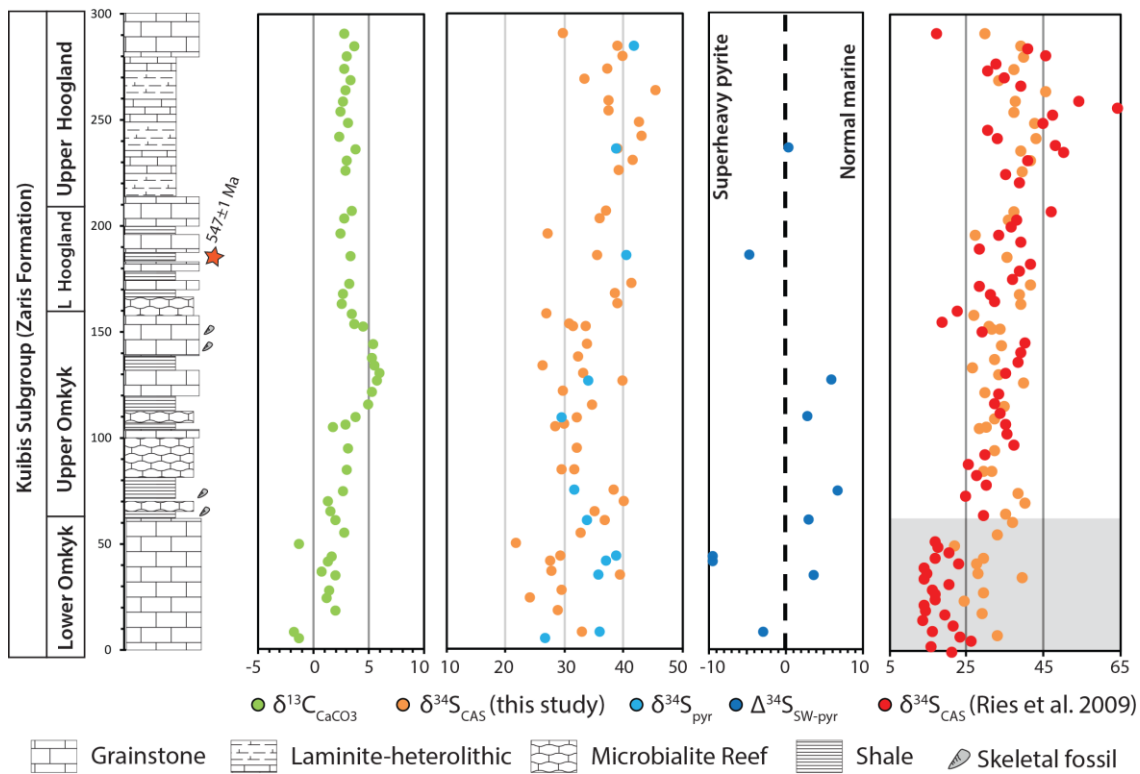
1210 Strauss, H., Bengtson, S., Myrow, P.M., Vidal, G., 1992. Stable isotope geochemistry  
 1211 and palynology of the late Precambrian to Early Cambrian sequence in  
 1212 Newfoundland. *Canadian Journal of Earth Sciences* 29, 1662–1673.  
 1213 Swart, P.K., Kennedy, M.J., 2012. Does the global stratigraphic reproducibility of  $\delta^{13}\text{C}$   
 1214 in Neoproterozoic carbonates require a marine origin? A Pliocene–  
 1215 Pleistocene comparison. *Geology* 40, 87–90. doi:10.1130/G32538.1  
 1216 Theiling, B.P., Coleman, M., 2015. Refining the extraction methodology of carbonate  
 1217 associated sulfate: Evidence from synthetic and natural carbonate samples.  
 1218 *Chemical Geology* 411, 36–48. doi:10.1016/j.chemgeo.2015.06.018  
 1219 Thode, H., Monster, J., 1965. Sulfur-isotope geochemistry of petroleum, evaporites,  
 1220 and ancient seas, in: *Fluids in Subsurfaces Environments: A Symposium*,  
 1221 *Memoir No. 4. American Association of Petroleum Geologists, AAPG Special*  
 1222 *Volumes*, pp. 367–377.  
 1223 Thode, H., Monster, J., Dunford, H., 1961. Sulphur isotope geochemistry. *Geochimica*  
 1224 *et Cosmochimica Acta* 25, 159–174. doi:10.1016/0016-7037(61)90074-6  
 1225 Tostevin, R., Wood, R.A., Shields, G.A., Poulton, S.W., Guilbaud, R., Bowyer, F., Penny,  
 1226 A.M., He, T., Curtis, A., Hoffmann, K.H., Clarkson, M.O., 2016. Low-oxygen  
 1227 waters limited habitable space for early animals. *Nature Communications* 7.  
 1228 doi:10.1038/ncomms12818  
 1229 Towe, K.M., 1970. Oxygen-Collagen Priority and the Early Metazoan Fossil Record.  
 1230 *PNAS* 65, 781–788.  
 1231 Turchyn, A.V., Schrag, D.P., Coccioni, R., Montanari, A., 2009. Stable isotope analysis  
 1232 of the Cretaceous sulfur cycle. *Earth and Planetary Science Letters* 285, 115–  
 1233 123. doi:10.1016/j.epsl.2009.06.002  
 1234 Wang, J., Chen, D., Yan, D., Wei, H., Xiang, L., 2012. Evolution from an anoxic to oxic  
 1235 deep ocean during the Ediacaran–Cambrian transition and implications for  
 1236 bioradiation. *Chemical Geology* 306–307, 129–138.  
 1237 doi:10.1016/j.chemgeo.2012.03.005  
 1238 Weber, H.S., Thamdrup, B., Habicht, K.S., 2016. High Sulfur Isotope Fractionation  
 1239 Associated with Anaerobic Oxidation of Methane in a Low-Sulfate, Iron-Rich  
 1240 Environment. *Front. Earth Sci* 461. doi:10.3389/feart.2016.00061  
 1241 Wilbanks, E.G., Jaekel, U., Salman, V., Humphrey, P.T., Eisen, J.A., Facciotti, M.T.,  
 1242 Buckley, D.H., Zinder, S.H., Druschel, G.K., Fike, D.A., Orphan, V.J., 2014.  
 1243 Microscale sulfur cycling in the phototrophic pink berry consortia of the  
 1244 Sippewissett Salt Marsh. *Environ Microbiol* 16, 3398–3415.  
 1245 doi:10.1111/1462-2920.12388  
 1246 Wood, R., A., 2011. Paleoecology of the earliest skeletal metazoan communities:  
 1247 Implications for early biomineralization. *Earth-Science Reviews* 106, 184–  
 1248 190. doi:10.1016/j.earscirev.2011.01.011  
 1249 Wood, R.A., Grotzinger, J.P., Dickson, J.A.D., 2002. Proterozoic Modular  
 1250 Biomineralized Metazoan from the Nama Group, Namibia. *Science* 296, 2383  
 1251 –2386. doi:10.1126/science.1071599  
 1252 Wood, R.A., Poulton, S.W., Prave, A.R., Hoffmann, K.-H., Clarkson, M.O., Guilbaud, R.,  
 1253 Lyne, J.W., Tostevin, R., Bowyer, F., Penny, A.M., Curtis, A., Kasemann, S.A.,  
 1254 2015. Dynamic redox conditions control late Ediacaran ecosystems in the  
 1255 Nama Group, Namibia. *Precambrian Research* 261, 252–271.

1256 Wortmann, U.G., Bernasconi, S.M., Böttcher, M.E., 2001. Hypersulfidic deep  
 1257 biosphere indicates extreme sulfur isotope fractionation during single-step  
 1258 microbial sulfate reduction. *Geology* 29, 647–650.  
 1259 Wotte, T., Shields-Zhou, G.A., Strauss, H., 2012. Carbonate-associated sulfate:  
 1260 experimental comparisons of common extraction methods and  
 1261 recommendations toward a standard analytical protocol. *Chemical Geology*  
 1262 326, 132–144.  
 1263 Wu, N., Farquhar, J., Fike, D.A., 2015. Ediacaran sulfur cycle: Insights from sulfur  
 1264 isotope measurements ( $\Delta^{33}\text{S}$  and  $\delta^{34}\text{S}$ ) on paired sulfate-pyrite in the Huqf  
 1265 Supergroup of Oman. *Geochimica et Cosmochimica Acta* 164, 352 - 364  
 1266 Zhang, T., Chu, X., Zhang, Q., Feng, L., Huo, W., 2004. The sulfur and carbon isotopic  
 1267 records in carbonates of the Dengying Formation in the Yangtze Platform,  
 1268 China. *Acta Petrologica Sinica* 20, 717–724.  
 1269 Zhang, T., Chu, X., Zhang, Q., Feng, L., Huo, W., 2003. Variations of sulfur and carbon  
 1270 isotopes in seawater during the Doushantuo stage in late Neoproterozoic.  
 1271 *Chin.Sci.Bull.* 48, 1375–1380. doi:10.1007/BF03184182  
 1272 Zhuravlev, A.Y., Wood, R.A., 2008. Eve of biomineralization: Controls on skeletal  
 1273 mineralogy. *Geology* 36, 923 –926. doi:10.1130/G25094A.1  
 1274  
 1275

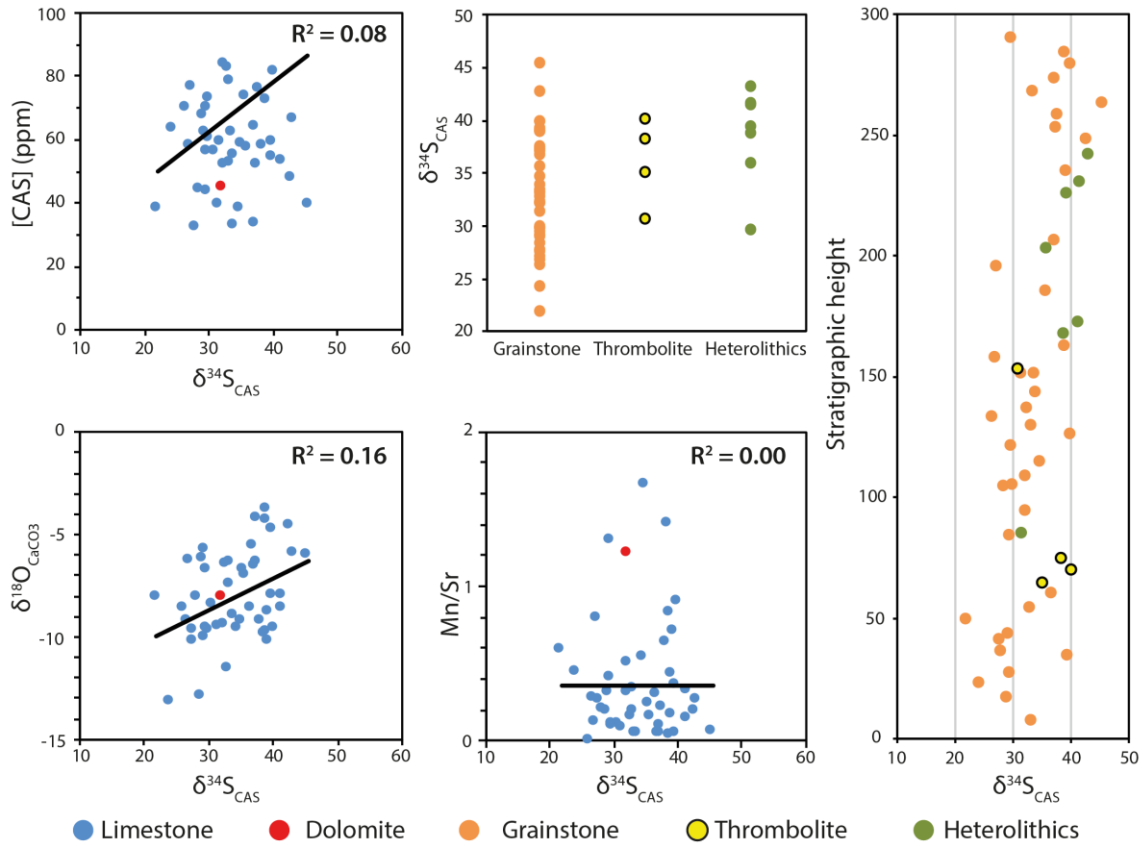
1276 **Figure 1:** Simplified geological map of Namibia, showing the location of Zebra River  
1277 section in the Kuibis Subgroup of the Nama Group, modified from Miller, (1983).



1281 **Figure 2:** The first panel shows carbon isotope ratios for carbonate rocks at Zebra  
 1282 River, Nama Group. In the second panel,  $\delta^{34}\text{S}_{\text{CAS}}$  from this study is shown alongside  
 1283  $\delta^{34}\text{S}_{\text{pyr}}$ . The third panel shows the isotope composition of CAS minus pyrite,  $\Delta^{34}\text{S}_{\text{SW-pyr}}$ .  
 1284  $\text{pyr}$ . The final panel shows sulfur isotope composition of CAS and pyrite from this  
 1285 study compared with equivalent parts of the stratigraphy from Ries et al. (2009). In  
 1286 the lower Omkyk, this study presents higher  $\delta^{34}\text{S}_{\text{SW}}$  than Ries et al. (2009) (grey  
 1287 box). Data from Ries et al. (2009) have been replotted on an equivalent depth scale  
 1288 using member boundaries.



1290 **Figure 3:**  $\delta^{34}\text{S}_{\text{CAS}}$  shows no correlation with traditional indicators of diagenesis, CAS  
 1291 concentration, Mn/Sr or  $\delta^{18}\text{O}_{\text{CaCO}_3}$ . In addition, the  $\delta^{34}\text{S}_{\text{CAS}}$  does not appear to follow  
 1292 lithological trends or facies changes.



1293

1294 **Figure 4:** Comparison of  $\delta^{34}\text{S}_{\text{CAS}}$  and  $\delta^{13}\text{C}$  data from carbonate successions from the  
1295 Buah Formation and Ara Group, Oman (Fike et al., 2006; Wu et al., 2015); the  
1296 Gaojiashan Member, south China (Cui et al., 2016) and the Nama Group, Namibia  
1297 (ths study). Radiometric age constraints and associated uncertainties are shown.  
1298 Potential tie points between Oman and the Nama Group (TP1-3) are referred to in  
1299 the text when discussing correlations between C and S isotope records.

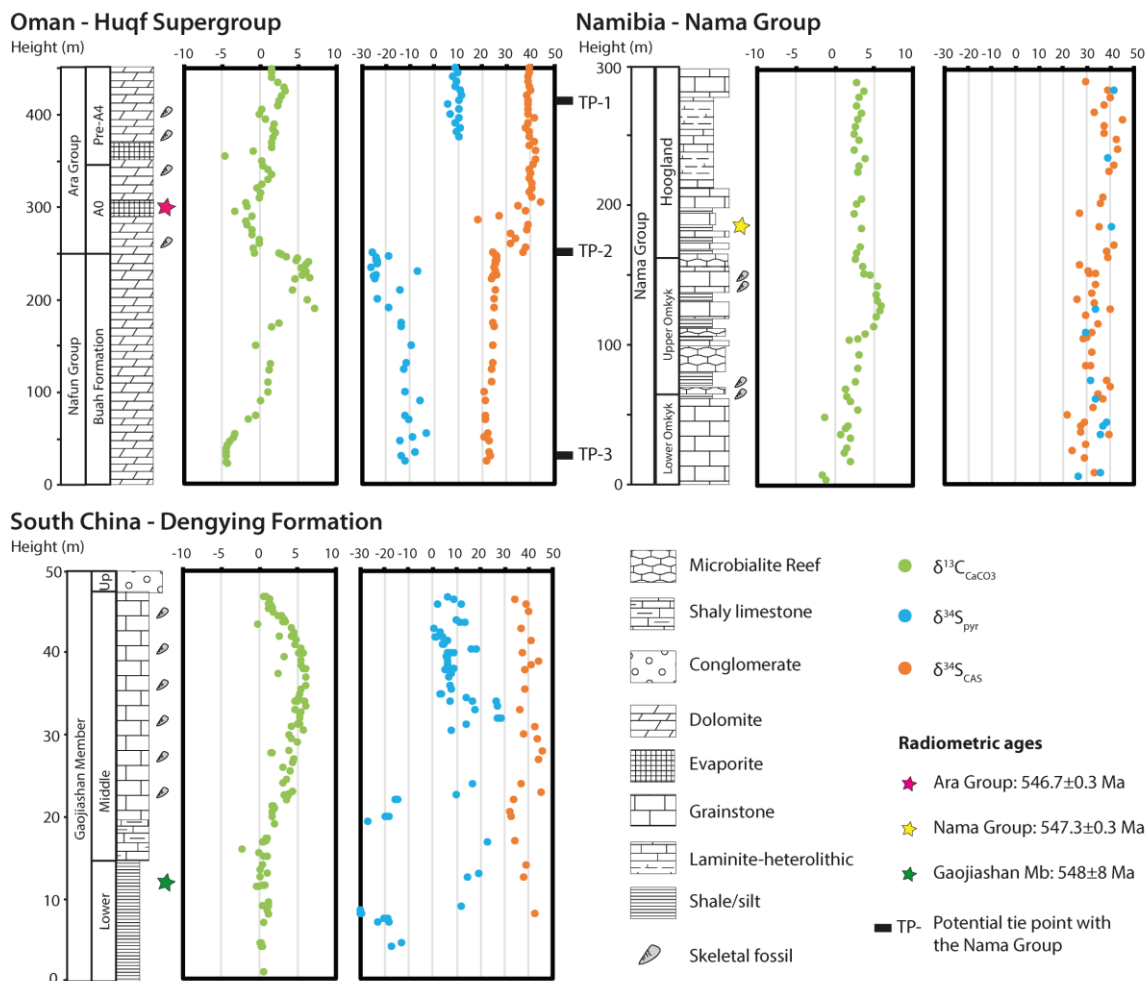


**Table 1:** Average sulfur isotope composition of CAS and pyrite in each member from this study and Ries et al. (2009), where 'n' indicates the number of analyses. Errors are one standard deviation. In the lower Omkyk, this study presents higher  $\delta^{34}\text{S}$  than Ries et al. (2009).

Member	Study	$\delta^{34}\text{S}$ CAS	$\delta^{34}\text{S}$ Pyrite	Pyrite compared with CAS
Lower Omkyk	This study	$30.1 \pm 5.1 \text{ ‰}$ (n=11)	$36.3 \pm 1.8 \text{ ‰}$ (n=5)	Some 'superheavy'
	Ries et al. 2009	$17.7 \pm 3.6 \text{ ‰}$	$28.7 \pm 4.0 \text{ ‰}$	
Upper Omkyk	This study	$32.5 \pm 3.8 \text{ ‰}$ (n=20)	$31.7 \pm 2.2 \text{ ‰}$ (n=3)	Similar
	Ries et al. 2009	$31.4 \pm 5.9 \text{ ‰}$	$29.9 \pm 5.9 \text{ ‰}$	
Hoogland	This study	$38.0 \pm 4.3 \text{ ‰}$ (n=20)	$40.4 \pm 1.5 \text{ ‰}$ (n= 3)	Some 'superheavy'
	Ries et al. 2009	$38.6 \pm 9.1 \text{ ‰}$	$40.9 \pm 12.7 \text{ ‰}$	

**Table 2:** Sulfur isotope ratios,  $\delta^{34}\text{S}$ , of the first two sodium chloride leachates compared with CAS for three selected samples. Leaches 3-5 did not produce sufficient precipitate for isotopic analysis. Pre-leaches shows lower  $\delta^{34}\text{S}$  compared with final CAS value, consistent with previous method development work by Wotte et al. (2012) and Peng et al., (2014).

Sample	$\delta^{34}\text{S}$ – Leach 1	$\delta^{34}\text{S}$ – Leach 2	$\delta^{34}\text{S}$ – CAS
UH11	35.2	22.3	33.4
UH5	38.1	34.4	39.1
UH14	23.1	-	38.9

1313